PROCEEDINGS OF THE ROYAL SOCIETY A MATHEMATICAL, PHYSICAL & ENGINEERING SCIENCES

On the Electrodynamic Balance

W. H. Hartung and C. T. Avedisian

Proc. R. Soc. Lond. A 1992 **437**, doi: 10.1098/rspa.1992.0060, published 8 May 1992

On the electrodynamic balance

By W. H. Hartung† and C. T. Avedisian

Sibley School of Mechanical and Aerospace Engineering, Cornell University, Ithaca, New York 14853-7501, U.S.A.

The properties of axially symmetric electrodynamic balances are studied using analytic and numerical techniques. The levitation ability and stability characteristics of several balance configurations are determined. A unified theory for the stability characteristics of all electrodynamic balances which have a non-vanishing quadrupole field term is derived. Procedures are proposed to optimize the balance shape for stably levitating particles of maximal mass to charge ratio. The lack of a unique optimum balance shape is demonstrated.

Nomenclature

a_j, b_j, c_j	coefficients in series expansion of the potential in spherical coordinates
A_j, B_j	dimensionless coefficients in series expansion of the potential in cylindrical coordinates
C_j	dimensionless coefficient in series expansion of the potential in spherical coordinates
$\partial v/\partial n$	normal derivative of the potential $\equiv \boldsymbol{n}\cdot\nabla v$
D_0	levitation design constant $\equiv z_c c_0/v_{\mathrm{end}}(t) = (z_c/z_0)\,C_0$
D_1	stabilization design constant $\equiv z_c^2 c_1/v_{\mathrm{ring}}(t) = (z_c/z_0)^2\,C_1$
$\boldsymbol{e}_r$	radial unit vector in cylindrical coordinates
$\boldsymbol{e}_s$	radial unit vector in spherical coordinates
$\boldsymbol{e}_z$	axial unit vector in cylindrical coordinates
$E_r(\boldsymbol{r}, t)$	radial component of the electric field
$E_z(\boldsymbol{r}, t)$	axial component of the electric field
$\boldsymbol{E}(\boldsymbol{r}, t)$	electric field
$\boldsymbol{E}_{\mathrm{i}}(\boldsymbol{r})$	electric field at $\boldsymbol{r}$ induced by a charged particle at $\boldsymbol{r}$
$\boldsymbol{E}_{\pm}(\boldsymbol{r}, t)$	even (+) or odd (−) parity component of the electric field
$f_n(\boldsymbol{r})$	function, $n = 0$ or 1
g	acceleration due to gravity
G	dimensionless gravitational acceleration parameter $\equiv g/z_0\,\Omega^2$
h	thickness of the ring electrode for the triple-disc shape
$J_n(x)$	Bessel function of the first kind of order n in x
$K(x)$	complete elliptic integral of the first kind in x
K_{D}	drag coefficient
L_{b}	radial and axial distance from the outside of the balance to the bounding cylinder for the double-ring/double-disc shape

† Present address: Department of Applied and Engineering Physics, Cornell University, Ithaca, New York 14853, U.S.A.

Proc. R. Soc. Lond. A (1992) **437**, 237–266
Printed in Great Britain

m	mass of the particle
$\mathscr{P}_j(x)$	Legendre polynomial in x of order j
q	particle charge
r	radial coordinate in the cylindrical coordinate system
r_r	half the thickness of the rings in the single-ring and double-ring shapes
r_s	radial coordinate in the spherical coordinate system
$r_{\mathrm{s}0}$	radius of the largest sphere that can be inscribed inside the balance electrodes
r_D	radius of the discs for the triple-disc shape
r_R	radius of the rings for the single-ring and double-ring shapes
r_0	distance from the origin to the ring electrode
$\boldsymbol{r}$	position vector
$\dot{\boldsymbol{r}}$	velocity vector
$\ddot{\boldsymbol{r}}$	acceleration vector
R	dimensionless radial coordinate in cylindrical coordinates $\equiv r/z_0$
R_ma	dimensionless radial distance to the end of the hyperboloidal electrodes
S_e	surface of the volume that electrodes must be outside of
$\mathscr{S}_j(x)$	second solution for the differential equation in θ
t	time
T	dimensionless time $\equiv \Omega t$
$v(\boldsymbol{r}, t)$	scalar electric potential
v_ac	amplitude of alternating potential applied to the ring electrode
v_dc	static potential applied to the ring electrode
$v_\mathrm{end}(t)$	half the potential difference applied across the endcap electrodes
$v_\mathrm{i}(\boldsymbol{r})$	electric potential induced by the charged particle
$v_\mathrm{ring}(t)$	potential applied to the ring electrode
$v_0(\boldsymbol{r})$	electric potential in the absence of the charged particle
$v_\pm(\boldsymbol{r}, t)$	even (+) or odd (−) parity component of the potential
$V_+(R, Z)$	dimensionless even parity component of potential $\equiv v_+(z_0 R, z_0 Z, t)/v_\mathrm{ring}(t)$
$V_-(R, Z)$	dimensionless odd parity component of potential $\equiv v_-(z_0 R, z_0 Z, t)/v_\mathrm{end}(t)$
x_j	jth zero of $J_0(x)$
z	axial coordinate in the cylindrical coordinate system
z_c	characteristic length defined from an excluded volume of given shape
z_R	half the distance between the rings for the double-ring and double-ring/cylinder shapes
z_0	characteristic dimension, usually equal to half the distance between the endcap electrodes along the z axis
Z	dimensionless axial coordinate in cylindrical coordinates $\equiv z/z_0$
α_k	coefficient in the series expansion for the potential in cylindrical coordinates
β_k	coefficient in the series expansion for the potential in cylindrical coordinates
δ	dimensionless drag parameter $\equiv K_\mathrm{D}/m\Omega$
ϵ_ac	dimensionless stabilizing field strength parameter $\equiv qv_\mathrm{ac}/mz_0^2\Omega^2$
ϵ'_ac	generalized dimensionless stabilizing field strength parameter $\equiv -2C_1 qv_\mathrm{ac}/mz_0^2\Omega^2 = -2C_1\epsilon_\mathrm{ac}$
ϵ_dc	dimensionless stabilizing field strength parameter $\equiv qv_\mathrm{ac}/mz_0^2\Omega^2$

ϵ'_{dc}	generalized dimensionless stabilizing field strength parameter $\equiv -2C_1 qv_{\mathrm{dc}}/mz_0^2\Omega^2 = -2C_1\epsilon_{\mathrm{dc}}$
$\epsilon_{\mathrm{end}}(T)$	dimensionless endcap field strength parameter $\equiv qv_{\mathrm{end}}(T/\Omega)/mz_0^2\Omega^2$
$\epsilon_{\mathrm{ring}}(T)$	dimensionless ring field strength parameter $\equiv qv_{\mathrm{ring}}(T/\Omega)/mz_0^2\Omega^2$
$\epsilon'_{\mathrm{ring}}(T)$	generalized ring field strength parameter $\equiv -2C_1 qv_{\mathrm{ring}}(T/\Omega)/mz_0^2\Omega^2 = -2C_1\epsilon_{\mathrm{ring}}(T)$
ϵ_0	permittivity of space
θ	polar angle in the spherical coordinate system
θ_m	parameter for the SVEL shape
θ_1	constant for the SVEL shape $\equiv \arccos(1/\sqrt{3}) = 54.74°$
λ	wavelength of plane electromagnetic wave propagation $\equiv 2\pi$ (speed of light)$/\Omega$
$\Xi_{\pm,r}(R,Z)$	dimensionless even (+) or odd (−) parity radial component of the electric field
$\Xi_{\pm,z}(R,Z)$	dimensionless even (+) or odd (−) parity axial component of the electric field
$\boldsymbol{\Xi}_{\mathrm{i}}(\boldsymbol{r})$	dimensionless electric field at $\boldsymbol{r}$ induced by a charged particle at $\boldsymbol{r}$
$\boldsymbol{\Xi}_+(R,Z)$	dimensionless even parity component of the electric field $\equiv z_0\boldsymbol{E}_+(z_0R, z_0Z, t)/v_{\mathrm{ring}}(t)$
$\boldsymbol{\Xi}_-(R,Z)$	dimensionless odd parity component of the electric field $\equiv z_0\boldsymbol{E}_-(z_0R, z_0Z, t)/v_{\mathrm{end}}(t)$
$\rho(\boldsymbol{r})$	charge density
$\sigma(\boldsymbol{r})$	surface charge density, i.e. charge per unit area on a surface
φ	azimuthal angle in the cylindrical and spherical coordinate systems
$\chi(\boldsymbol{r})$	proportionality factor relating $\sigma(\boldsymbol{r})$ to $v(\boldsymbol{r})$ = normalized capacitance per unit area
Ω	angular frequency of the alternating potential

1. Introduction

The electrodynamic balance, also referred to as an electrodynamic trap, an electrodynamic containment chamber, an electrodynamic levitator and a quadrupole has been the object of growing interest in recent years. It has been used in the study of a wide variety of subjects, including mass transfer, charge transfer, heat transfer, charge stability, aerodynamic drag, crystallization, photoemission and molecular spectroscopy, among many others. More recently, the balance has been used to study combustion for mechanical engineering applications (see, for example, Spjut *et al.* 1986; Phuoc & Maloney 1988). Several reviews of the development and applications of the electrodynamic balance can be found in the literature (Davis 1983, 1987; Straubel & Straubel 1986). An instrument for stored ion spectroscopy has also been developed by combining the balance with magnetic confinement (see, for example, Wineland *et al.* 1983).

The development of the balance can be traced back to Millikan's oil drop experiment, in which a charged particle is suspended electrostatically between two electrodes, one above and the other below it (see, for example, Millikan 1917). Stable levitation of particles, as a consequence of the Earnshaw theorem (see, for example, Maxwell 1892), however, is not possible in a purely electrostatic field. Good (1953) proposed a particle suspension system which would use a time-varying electric field

in a manner similar to the alternating gradient focusing system developed by Courant *et al.* (1952) for charged particle beams. Subsequently, charged particles were suspended dynamically in a sinusoidally varying electric field produced by a ring-shaped electrode (Straubel 1955, 1956). The principles of operation of an electric mass filter (Paul & Raether 1955) were next used to combine the dynamic stabilization of the ring electrode with Millikan levitation produced by two endcap electrodes, giving birth to the modern-day electrodynamic balance (Wuerker *et al.* 1959). Solid particles and liquid droplets in the size range of roughly 0.3 μm to 300 μm have been suspended in such balances.

A distinguishing feature of an electrodynamic balance is the contour of the balance electrodes; a few of the possible balance shapes are shown in figure 1. A number of investigators have analysed various balance shapes and examined their levitation ability. Stability analysis is more involved, and the stability characteristics of only a handful of balance shapes are well understood.

In this paper, a general stability theory for electrodynamic balances will be derived and applied to identify balance configurations that are optimal for stable levitation of particles with large masses and small charges. The theory of the electrodynamic balance will first be briefly reviewed. A generalization of existing stability theories for specific balance shapes will then be shown to apply to all balance shapes with axial symmetry and a quadrupole electrostatic field component. The electric fields and shape constants will be calculated numerically for some different electrode configurations and an analytic solution for a new balance shape will be given; the stability and levitation characteristics of these balance shapes will be compared with known results. Finally, the existence of classes of optimum balances and the nonexistence of a unique optimum balance shape will be demonstrated.

2. Theory

An electrodynamic balance must (i) levitate a particle and (ii) keep it stable. The equations of motion for a particle travelling inside the balance determine its performance. Assuming a non-relativistic velocity, the particle's motion is governed by Newton's second law, for which the electromagnetic force on the particle is needed. We first review the theory of electrostatics briefly, and then derive the general equations of motion for a particle in a balance. We use these equations to analyse levitation, and then show that they can be linearized to obtain a general stability theory applicable to all balance shapes.

(*a*) *Electrostatics*

In the absence of significant external magnetic fields and when the time variation in the charge density ρ is sufficiently slow, electrodynamics reduces to electrostatics. The Maxwell equations in potential form then reduce to the Poisson equation

$$\nabla^2 v = -(1/\epsilon_0)\rho, \tag{1}$$

which relates the scalar electric potential v to the charge density ρ. The electric field $\boldsymbol{E}$ is given in terms of v by

$$\boldsymbol{E} = -\nabla v. \tag{2}$$

When ρ is varying in time, (1) and (2) do not apply exactly. For example, when ρ varies sinusoidally in time, the relative error in v that results from assuming ρ to be

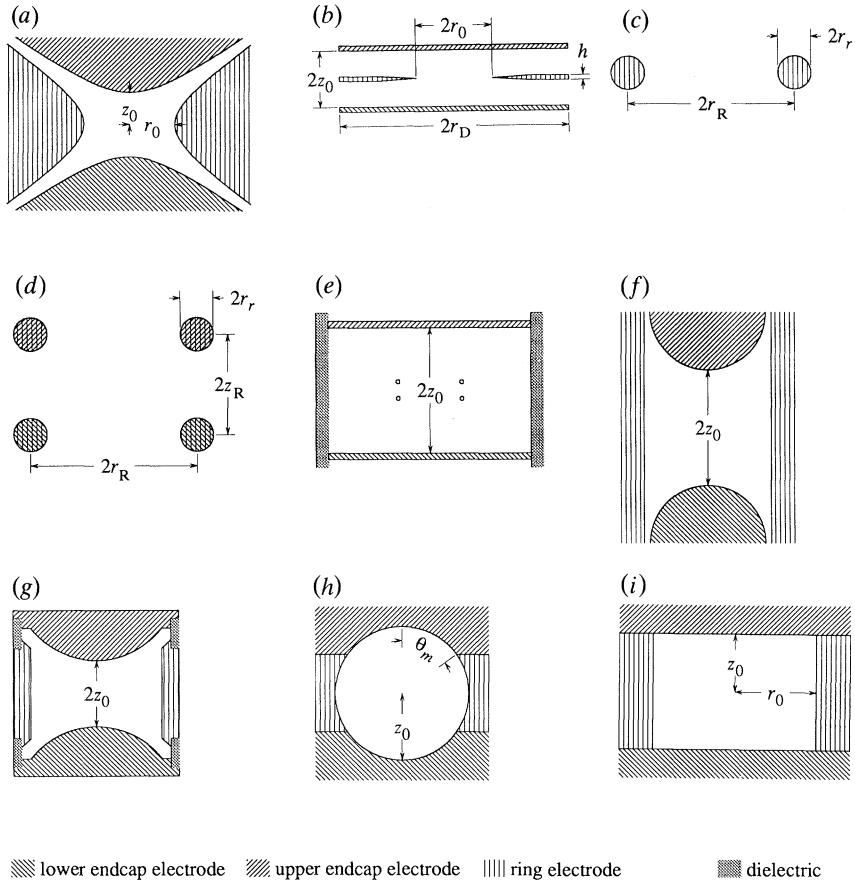

Figure 1. Sectional view of some possible electrode configurations for an electrodynamic balance. All shapes are axisymmetric. (*a*) Ideal hyperboloidal electrodes (surfaces extend to infinity). The ring electrode satisfies $r^2-2z^2 = r_0^2$; the endcap electrodes satisfy $r^2-2z^2 = 2z_0^2$. (*b*) One form of the 'triple-disc' configuration (Ataman & Hanson 1969). (*c*) Single-ring configuration (Müller 1960). This shape does not incorporate electrodes for balancing gravity, so it can only suspend particles in dynamic equilibrium. (*d*) Double-ring configuration (Berg *et al.* 1970; Davis *et al.* 1990). (*e*) Double-ring/double-disc configuration (Weiss-Wrana 1983; Ward 1989). This shape is usually called a double-ring balance. (*f*) Spherical endcap electrodes and a cylindrical ring electrode (Berg & Gaukler 1969). (*g*) Bihemispherical configuration (Richardson & Spann 1984). (*h*) Spherical void (SVEL) configuration (Arnold & Folan 1987). (*i*) 'Pillbox' configuration.

static is of the order of $z_0^2/(\lambda^2+z_0^2)$, where z_0 is the characteristic length over which v varies spatially. For an electrodynamic balance, z_0 is typically of the order of 1 cm and the frequency is typically of the order of 100 Hz, in which case the relative error in v is about 10^{-17}. The error becomes significant at sufficiently high frequencies, however.

Equation (1) reduces to the Laplace equation,

$$\nabla^2 v = 0, \tag{3}$$

in regions where ρ is zero. In an electrodynamic balance, this condition is satisfied everywhere inside the volume bounded by the electrodes except at the location of the levitated particle. Neglecting the effect of the particle's charge makes the calculation

of v much more tractable, so ρ will be assumed to be zero everywhere inside the balance and (3) will then apply everywhere inside the balance. The validity of this idealization is examined in Appendix A.

When solving (3), it is useful to think in terms of boundary conditions on v produced by ρ rather than solving for v as a functional of ρ. The requirement that ρ be slowly varying in time becomes the requirement that the boundary conditions be slowly time varying. Boundary conditions on the electrode surfaces (and at infinity, if necessary) determine a unique solution for v. For perfectly conducting electrodes, v is constant on an electrode surface (Dirichlet boundary condition). Another permissible boundary condition, which can sometimes be applied by symmetry, is that $\partial v/\partial n = 0$, i.e. the electric field is tangent to the surface (Neumann boundary condition).

When a medium other than vacuum is present, additional bound charge may exist on its boundaries. The normal component of $\boldsymbol{E}$ is discontinuous due to the bound charge at the interface between two media of different dielectric constant (for isotropic linear media). For air, the dielectric correction is usually negligible, but for media such as insulators, it can be significant. Dielectric regions are included in some of the calculations discussed herein.

(*b*) *Electrostatics applied to the electrodynamic balance*

To derive the series expressions for the potential and fields in a balance, we follow essentially the established procedure (Frickel *et al.* 1978; Davis 1985), but use a slightly different approach to facilitate the subsequent analysis. We consider an electrode configuration consisting of two endcap electrodes, across which a static potential difference may be established to provide an upward force on the levitated particle, and a ring electrode, to which a stabilizing potential may be applied, and impose the following restrictions: (i) the electrodes are axisymmetric, so that the potential in cylindrical coordinates (r, z, φ) is independent of φ; (ii) the origin of coordinates is inside the balance (not inside an electrode) and the potential is finite in some open region containing the origin; and (iii) the electrode configuration is symmetric under reflection about the $z = 0$ plane.

Restriction (i) implies that v depends only on r, z and t. For an axisymmetric problem, writing (3) in spherical coordinates (r_s, θ, φ) and separating variables yields a general solution for v in terms of Legendre polynomials and another set of orthogonal functions (Frickel *et al.* 1978):

$$v(r_s, \theta) = \sum_{j=-1}^{\infty} \left(c_j r_s^{j+1} + \frac{b_j}{r_s^{j+2}} \right) [\mathscr{P}_{j+1}(\cos\theta) + a_j \mathscr{S}_{j+1}(\theta)]. \tag{4}$$

The starting value $j = -1$ is used here because the first term in the series does not contribute to the electrodynamic force, as will become evident later on.

Restriction (ii) requires that all of the b_j and a_j coefficients in (4) vanish. Transformation of the remaining terms into cylindrical coordinates yields an infinite series in terms of harmonic polynomials:

$$\begin{aligned} v(r, z, t) = {} & c_{-1} + c_0 z + c_1(z^2 - \tfrac{1}{2}r^2) + c_2(z^3 - \tfrac{3}{2}zr^2) + c_3(z^4 - 3z^2r^2 + \tfrac{3}{8}r^4) \\ & + c_4(z^5 - 5z^3r^2 + \tfrac{15}{8}zr^4) + c_5(z^6 - \tfrac{15}{2}z^4 r^2 + \tfrac{45}{8}z^2r^4 - \tfrac{5}{16}r^6) \\ & + c_6(z^7 - \tfrac{21}{2}z^5r^2 + \tfrac{105}{8}z^3r^4 - \tfrac{35}{16}zr^6) + \ldots . \end{aligned} \tag{5}$$

The potential can depend on t because of the possible time dependence in the

boundary conditions, and hence in the c_j coefficients. It is convenient to resolve v into the sum of two functions of opposite parity:

$$v(r,z,t) = v_+(r,z,t) + v_-(r,z,t), \tag{6}$$

where $v_+(r,z,t) = v_+(r,-z,t)$ is an even parity solution to the Laplace equation and $v_-(r,z,t) = -v_-(r,-z,t)$ is an odd parity solution. It is evident from (5) that $v_+(r,z,t)$ will contain only the terms in the series for $v(r,z,t)$ with even powers of z and $v_-(r,z,t)$ will contain only the terms with odd powers of z. Associated with v_+ and v_- are two components of the electric field, $\boldsymbol{E}_+ = -\nabla v_+$ and $\boldsymbol{E}_- = -\nabla v_-$.

With one ring electrode and two endcap electrodes, the boundary conditions for $v(r,z,t)$ can, in general, be set up by applying three independent potentials to the three electrodes. However, because the electric field depends only on the gradient of v, we are free to choose an arbitrary reference potential. It is convenient to choose this reference potential to be the average of the two potentials applied to the endcaps and to set to it equal to zero. Then only two potentials remain: if potentials $v_{\text{ring}}(t)$ and $v_{\text{end}}(t)$ are applied to the ring electrode and the upper endcap electrode, respectively, the potential applied to the lower endcap electrode is $-v_{\text{end}}(t)$. Because the Laplace equation is linear, the potential $v(r,z,t)$ corresponding to these boundary conditions can be obtained by first solving for the potential with $v_{\text{end}}(t)$ set to 0, then solving for the potential with $v_{\text{ring}}(t)$ set to 0, and finally adding these two potentials to get the actual result. Restriction (iii) implies that the potential must have even parity when $v_{\text{end}}(t) = 0$ and odd parity when $v_{\text{ring}}(t) = 0$; hence the two components of the potential are just $v_+(r,z,t)$ and $v_-(r,z,t)$.

Dimensionless coordinates R and Z can be defined in terms of the distance z_0 to the endcap electrodes along the z axis. Similarly, the two components v_+ and v_- of v can be normalized using $v_{\text{ring}}(t)$ and $v_{\text{end}}(t)$ to obtain dimensionless potential components $V_+(R,Z)$ and $V_-(R,Z)$. The linearity of the Laplace equation guarantees that if $V_+(R,Z)$ is 1 on the surface of the ring electrode and 0 on the surface of the endcap electrodes, then $v_+(r,z,t)$ will satisfy the requirements given above; likewise the requirements for $v_-(r,z,t)$ will be satisfied if $V_-(R,Z)$ is 0 on the surface of the ring electrode, 1 on the surface of the upper endcap electrode, and -1 on the surface of the lower endcap electrode. The problem of finding $v(r,z,t)$ subject to three arbitrary time-dependent potentials is thus reduced to the problem of finding $V_+(R,Z)$ and $V_-(R,Z)$ under the time-independent boundary conditions just stated, with the full time-dependent potential given by

$$v(r,z,t) = v_{\text{ring}}(t)\, V_+(r/z_0, z/z_0) + v_{\text{end}}(t)\, V_-(r/z_0, z/z_0). \tag{7}$$

Equation (5) can be resolved into components and non-dimensionalized to obtain series expressions for V_+ and V_-:

$$V_+(R,Z) = C_{-1} + C_1(Z^2 - \tfrac{1}{2}R^2) + C_3(Z^4 - 3Z^2R^2 + \tfrac{3}{8}R^4) + C_5(Z^6 - \tfrac{15}{2}Z^4R^2 + \tfrac{45}{8}Z^2R^4 - \tfrac{5}{16}R^6) + \ldots, \tag{8}$$

$$V_-(R,Z) = C_0 Z + C_2(Z^3 - \tfrac{3}{2}ZR^2) + C_4(Z^5 - 5Z^3R^2 + \tfrac{15}{8}ZR^4) + C_6(Z^7 - \tfrac{21}{2}Z^5R^2 + \tfrac{105}{8}Z^3R^4 - \tfrac{35}{16}ZR^6) + \ldots, \tag{9}$$

with the coefficients defined by

$$C_j = \begin{cases} z_0^{j+1}\, c_j / v_{\text{ring}}(t) & \text{for } j \text{ odd}, \\ z_0^{j+1}\, c_j / v_{\text{end}}(t) & \text{for } j \text{ even}. \end{cases} \tag{10}$$

It is also useful to transform from $\boldsymbol{E}_+$ and $\boldsymbol{E}_-$ to the dimensionless electric field components $\boldsymbol{\Xi}_+$ and $\boldsymbol{\Xi}_-$ defined in terms of $v_{\mathrm{ring}}(t)$, $v_{\mathrm{end}}(t)$ and z_0. Series expressions for $\boldsymbol{\Xi}_+$ and $\boldsymbol{\Xi}_-$ can be obtained by differentiating (8) and (9) using (2), which yields

$$\boldsymbol{\Xi}_+(R,Z) = [C_1 R + 3C_3(2Z^2R - \tfrac{1}{2}R^3) + 15C_5(Z^4R - \tfrac{3}{2}Z^2R^3 + \tfrac{1}{8}R^5) + \ldots]\,\boldsymbol{e}_r - [2C_1 Z + 2C_3(2Z^3 - 3ZR^2) + 3C_5(2Z^5 - 10Z^3R^2 + \tfrac{15}{4}ZR^4) + \ldots]\,\boldsymbol{e}_z, \quad (11)$$

$$\boldsymbol{\Xi}_-(R,Z) = [3C_2 ZR + 5C_4(2Z^3R - \tfrac{3}{2}ZR^3) + \ldots]\,\boldsymbol{e}_r - [C_0 + 3C_2(Z^2 - \tfrac{1}{2}R^2) + 5C_4(Z^4 - 3Z^2R^2 + \tfrac{3}{8}R^4) + \ldots]\,\boldsymbol{e}_z. \quad (12)$$

The electrostatics problem is solved by finding the potential $v(r,z,t)$ inside the balance, which, as shown above, can be done by finding $V_+(R,Z)$ and $V_-(R,Z)$ and then obtaining $v(r,z,t)$ using (7). If all the series coefficients C_j can be calculated, V_+ and V_- can be obtained from (8) and (9). Expressing the solution in terms of these coefficients is useful in analysing the motion, as will be discussed below. Known results expressed in terms of the series coefficients are summarized in table 1. The two most popular shapes are the hyperboloidal shape (figure 1*a*), for which all the odd coefficients in the potential expansion after C_1 are zero in the ideal case, and the triple-disc shape (figure 1*b*), for which all the even coefficients in the potential expansion after C_0 are zero in the ideal case.

(*c*) *Equations of motion*

The first step in stability analysis, formulation of the general equations of motion for a particle in the electrodynamic balance, will now be reviewed in preparation for the derivation of a unified stability theory. It is also possible to simplify the equations of motion by assuming a rapid, small-scale oscillation superposed upon a slower, large-scale motion (Wuerker *et al.* 1959; Richardson & Spann 1984; Arnold & Hessel 1985; Arnold & Folan 1987). The approximate theory gives insight into the dynamics of trapping the particle, but because it applies only for small-amplitude stabilizing potentials, it is no substitute for the full analysis which we will discuss.

The electric force on a particle can be obtained by finding $V_+(R,Z)$ and $V_-(R,Z)$, calculating v using (7), and obtaining $\boldsymbol{E}$ from (2). The force on a particle of charge q at position $\boldsymbol{r}$ at time t is then $q\boldsymbol{E}(\boldsymbol{r},t)$. The gravitational force is $-mg\,\boldsymbol{e}_z$ for a particle of mass m when the z axis is directed vertically upward. The aerodynamic drag force will be expressed as $-K_{\mathrm{D}}\dot{\boldsymbol{r}}$, with the drag coefficient K_{D} assumed constant (the stokesian low velocity limit); correction terms must be included for large velocities, but numerical analysis has shown that the high Reynolds number correction to the drag is unimportant in a typical electrodynamic balance (Ataman & Hanson 1969).

Under the above assumptions, the vector equation of motion for a particle can be written as

$$m\ddot{\boldsymbol{r}} = q\boldsymbol{E}(\boldsymbol{r},t) - mg\,\boldsymbol{e}_z - K_{\mathrm{D}}\dot{\boldsymbol{r}} \quad (13)$$

(buoyancy, drag due to a uniform fluid flow, and other position-independent and time-independent vertical forces can be easily incorporated by proper redefinition of the mg term).

In cylindrical coordinates, the three vector components of (13) are

$$m(\ddot{r} - r\dot{\varphi}^2) = qE_r(r,z,t) - K_{\mathrm{D}}\dot{r}, \quad (14)$$

$$m\ddot{z} = qE_z(r,z,t) - mg - K_{\mathrm{D}}\dot{z}, \quad (15)$$

$$m(r\ddot{\varphi} + 2\dot{r}\dot{\varphi}) = -K_{\mathrm{D}}\,r\dot{\varphi}. \quad (16)$$

Table 1. *Theoretical values of series coefficients*

analytic results

balance shape	C_0	C_1	C_j for j even	C_j for j odd
parallel plates	1	0	0	0
hyperboloidal (Frickel *et al.* 1978)	—	$-1/(1+\frac{1}{2}(r_0/z_0)^2)$	—	0
hyperboloidal $r_0/z_0=\infty$ (Davis 1985)	$1/\sqrt{3}\ \ln\ (\sqrt{2}/(\sqrt{3}-1))$ $=0.876794$	0	$C_0/3^j(j+1)$	0
triple-disc $r_D \gg z_0$, $h=0$ (Müller 1960)	1	—	0	—
SVEL (Arnold & Folan 1987)	$\frac{3}{2}\sin^2\theta_m$	$-\frac{5}{2}\cos\theta_m \sin^2\theta_m$	$\mathscr{P}_j(\cos\theta_m)-\mathscr{P}_{j+2}(\cos\theta_m)$	$\mathscr{P}_{j+2}(\cos\theta_m)-\mathscr{P}_j(\cos\theta_m)$

balance shape	C_0	C_1	C_2	C_3	C_4
triple-disc[a] $r_D \gg z_0$, $h=0$, $r_0 \ll z_0$ (Müller 1960)	1	$-\frac{2}{\pi}\frac{z_0}{r_0}$	0	$\frac{2}{3\pi}\left(\frac{z_0}{r_0}\right)^3$	0
single ring[a] $r_r \ll r_R$, $z_0 \equiv r_R$ (Müller 1960)	0	$-\frac{1}{2}\pi\frac{1}{\ln(8r_R/r_r)}$	0	$-\frac{3\pi}{8}\frac{1}{\ln(8r_R/r_r)}$	0
double-ring $r_R/r_R=\frac{5}{4}$, $z_r/z_R=\frac{3}{16}$, $z_0 \equiv z_R$ (Berg *et al.* 1970)	0.80[b]	—	—	—	—

balance shape	C_0	C_1
double-ring $r_r \ll z_R$, $r_r \ll r_R$ $z_0 \equiv z_R$ (Davis *et al.* 1990)	$2\pi\Big/\left\{\left[1+\left(\frac{r_R}{z_R}\right)^2\right]\sqrt{\left(1+\left(\frac{z_R}{r_R}\right)^2\right)}K\left(1-\left(\frac{r_r}{4r_R}\right)^2\right)$ $-K\left(1-\left(\frac{r_r}{4r_R}\right)^2-\left(\frac{z_R}{r_R}\right)^2\right)\right\}$	$-\pi\Big/\left\{\left[1+\left(\frac{r_R}{z_R}\right)^2\right]\sqrt{\left(1+\left(\frac{z_R}{r_R}\right)^2\right)}K\left(1-\left(\frac{r_r}{4r_R}\right)^2\right)$ $+K\left(1-\left(\frac{r_r}{4r_R}\right)^2-\left(\frac{z_R}{r_R}\right)^2\right)\right\}$

numerical results (see also Sloane & Elmoursi 1987)

balance shape	C_0	C_1
hyperboloidal, $r_0/z_0=\sqrt{2}$ (Philip 1981)	0.800 ± 0.008[c]	—
triple-disc, $r_0/z_0=\frac{4}{3}$ (Ataman & Hanson 1969)	—	-0.368[d]

[a] From the definition of α, β, q, and $F(q)$. [b] From the result $k_{dc}=3.3\ (10^5)$. [c] From the result $C\approx 0.4$ with error of about 1%. [d] From the result $C=1.31$.

Equation (16) describes exponential decay of the angular momentum of the particle about the z axis. If $\dot{\varphi}$ is initially zero, φ is a constant of the motion and the φ term in (14) drops out. In this analysis, the motion will be assumed be to confined to a plane of constant φ, although motion in the φ direction could be excited by injecting the particle with a velocity component normal to the rz plane.

The equations of motion can be non-dimensionalized using the dimensionless coordinates R and Z, the dimensionless fields $\boldsymbol{\Xi}_+$ and $\boldsymbol{\Xi}_-$, and a dimensionless time $T = \Omega t$, where Ω is a characteristic angular frequency. With $\dot{\varphi} = 0$, (14) and (15) become

$$\mathrm{d}^2R/\mathrm{d}T^2 = \epsilon_{\mathrm{ring}}(T)\,\boldsymbol{\Xi}_{+,r}(R,Z) + \epsilon_{\mathrm{end}}(T)\,\boldsymbol{\Xi}_{-,r}(R,Z) - \delta\,\mathrm{d}R/\mathrm{d}T, \tag{17}$$

$$\mathrm{d}^2Z/\mathrm{d}T^2 = \epsilon_{\mathrm{ring}}(T)\,\boldsymbol{\Xi}_{+,z}(R,Z) + \epsilon_{\mathrm{end}}(T)\,\boldsymbol{\Xi}_{-,z}(R,Z) - G - \delta\,\mathrm{d}Z/\mathrm{d}T. \tag{18}$$

Equations (17) and (18) are the governing equations for levitation and stability.

(*d*) *Levitation*

When the particle is motionless, (17) and (18) reduce to

$$\epsilon_{\mathrm{ring}}(T)\,\boldsymbol{\Xi}_{+,r}(R,Z) + \epsilon_{\mathrm{end}}(T)\,\boldsymbol{\Xi}_{-,r}(R,Z) = 0, \tag{19}$$

$$\epsilon_{\mathrm{ring}}(T)\,\boldsymbol{\Xi}_{+,z}(R,Z) + \epsilon_{\mathrm{end}}(T)\,\boldsymbol{\Xi}_{-,z}(R,Z) - G = 0. \tag{20}$$

Equations (11) and (12) suggest that the origin might be a good location for levitating the particle since $\boldsymbol{\Xi}_+ = 0$ and $\boldsymbol{\Xi}_- = -C_0\,\boldsymbol{e}_z$ there. At the origin, (19) is satisfied automatically and (20) is satisfied if

$$\epsilon_{\mathrm{end}}(T) = -G/C_0, \tag{21}$$

or, in dimensional form, if

$$v_{\mathrm{end}}(t) = -mgz_0/qC_0. \tag{22}$$

A particle can thus be levitated at the point $R = 0$, $Z = 0$ (the 'null point' of the balance) by applying a static potential given by (22) across the endcap electrodes; the coefficient C_0 is a scale-independent measure of the levitation ability of a balance, and will be called the 'levitation strength constant' of a balance.

(*e*) *A unifying stability theory*

A particle is stably levitated in a balance if the solutions $R(T)$ and $Z(T)$ to (17) and (18) go to 0 as $T \to \infty$. Solutions to (17) and (18) depend on the balance shape because of the presence of the shape-dependent fields $\boldsymbol{\Xi}_+(R,Z)$ and $\boldsymbol{\Xi}_-(R,Z)$ in (17) and (18). To obtain particle trajectories for more than one balance shape, one must in general analyse each shape separately. For stability, however, only small perturbations from equilibrium need be considered. We will now show that, in the limit of small perturbations, the formerly shape-specific solutions to (17) and (18) become *unique* and applicable to *all* balance shapes with non-zero C_1, hence the notion of a 'unifying stability theory'. The existence of such a theory has been suggested or implied in prior work (Müller 1960; Ward 1989). This section will show that a unified stability theory does in fact exist, as a consequence of the form assumed by the equations of motion for small perturbations from the null point.

In the limit of small perturbations from the null point, (11) and (12) reduce to

$$\boldsymbol{\Xi}_+(R,Z) = C_1(R\,\boldsymbol{e}_r - 2Z\,\boldsymbol{e}_z), \tag{23}$$

$$\boldsymbol{\Xi}_-(R,Z) = -C_0\,\boldsymbol{e}_z. \tag{24}$$

Substituting (23) and (24) into (17) and (18) and using (21) to correctly balance the gravitational force yields

$$\mathrm{d}^2R/\mathrm{d}T^2+\delta\,\mathrm{d}R/\mathrm{d}T-\epsilon_{\mathrm{ring}}(T)\,C_1R=0, \tag{25}$$

$$\mathrm{d}^2Z/\mathrm{d}T^2+\delta\,\mathrm{d}Z/\mathrm{d}T+2\epsilon_{\mathrm{ring}}(T)\,C_1Z=0. \tag{26}$$

In contrast to (17) and (18), in which the shape-dependent fields $\Xi_+(R,Z)$ and $\Xi_-(R,Z)$ appear, (25) and (26) contain no unknown functions of R and Z. Equations (25) and (26) can consequently be solved without choosing a specific balance shape; the only needed parameters are δ, $\epsilon_{\mathrm{ring}}(T)$, and C_1, and these can all be taken to be independent parameters (unlike $\Xi_+(R,Z)$ and $\Xi_-(R,Z)$, which are rather difficult to treat as independent). Thus, in contrast to (17) and (18), general solutions $R(T,\delta,C_1,[\epsilon_{\mathrm{ring}}])$ and $Z(T,\delta,C_1,[\epsilon_{\mathrm{ring}}])$ to (25) and (26) can be found (the brackets indicate that R and Z are functionals of $\epsilon_{\mathrm{ring}}(T)$). Since the stability characteristics follow directly from the solutions to (25) and (26), unique stability results that apply to all balances will emerge from solutions to (25) and (26). The balance shape affects the motion, and hence stability, only through C_1, which will be called the 'stabilization strength constant' of a balance. The value of C_1 for a particular balance shape must still be obtained by solving (3).

The coefficient C_1 appears only as a factor in the product $\epsilon_{\mathrm{ring}}(T)\,C_1$ in both (25) and (26), so it can be incorporated into a generalized parameter $\epsilon'_{\mathrm{ring}}(T)$, with the result

$$\mathrm{d}^2R/\mathrm{d}T^2+\delta\,\mathrm{d}R/\mathrm{d}T+\tfrac{1}{2}\epsilon'_{\mathrm{ring}}(T)\,R=0 \tag{27}$$

$$\mathrm{d}^2Z/\mathrm{d}T^2+\delta\,\mathrm{d}Z/\mathrm{d}T-\epsilon'_{\mathrm{ring}}(T)\,Z=0. \tag{28}$$

Equations (27) and (28) have general solutions $R(T,\delta,[\epsilon'_{\mathrm{ring}}])$ and $Z(T,\delta,[\epsilon'_{\mathrm{ring}}])$, so that stability depends only on δ and $\epsilon'_{\mathrm{ring}}(T)$. Once obtained, the general solutions can be applied to any specific balance by using the value of C_1 for that balance to convert from $\epsilon'_{\mathrm{ring}}(T)$ to $\epsilon_{\mathrm{ring}}(T)$. Likewise, results for a specific balance shape can be generalized using the C_1 value for that balance to convert from $\epsilon_{\mathrm{ring}}(T)$ to $\epsilon'_{\mathrm{ring}}(T)$. This result applies to all balances with $C_1\neq 0$. When $C_1=0$, (23) gives $\Xi_+(R,Z)=0$, and the next term in the expansion becomes important.

To solve (27) and (28), the time dependence of $\epsilon'_{\mathrm{ring}}(T)$, i.e. of $v_{\mathrm{ring}}(t)$, must be chosen. The conventional choice is to apply a potential to the ring electrode of the form

$$v_{\mathrm{ring}}(t)=v_{\mathrm{dc}}+v_{\mathrm{ac}}\cos\Omega t. \tag{29}$$

By defining suitable dimensionless parameters ϵ_{dc} and ϵ_{ac} and their generalized counterparts ϵ'_{dc} and ϵ'_{ac}, we can write $\epsilon'_{\mathrm{ring}}(T)=\epsilon'_{\mathrm{dc}}+\epsilon'_{\mathrm{ac}}\cos T$. Equations (27) and (28) then become

$$\mathrm{d}^2R/\mathrm{d}T^2+\delta\,\mathrm{d}R/\mathrm{d}T+\tfrac{1}{2}(\epsilon'_{\mathrm{dc}}+\epsilon'_{\mathrm{ac}}\cos T)\,R=0, \tag{30}$$

$$\mathrm{d}^2Z/\mathrm{d}T^2+\delta\,\mathrm{d}Z/\mathrm{d}T-(\epsilon'_{\mathrm{dc}}+\epsilon'_{\mathrm{ac}}\cos T)\,Z=0. \tag{31}$$

The three dimensionless parameters governing stability in (30) and (31) are δ (proportional to the drag coefficient), ϵ'_{dc} (proportional to the static potential applied to the ring), and ϵ'_{ac} (proportional to the alternating potential applied to the ring). For given values of these three parameters, a particle's motion is either stable or unstable. An understanding of the stability characteristics of a balance implies knowing where the particle's motion is stable and where it is unstable in the $\delta\epsilon'_{\mathrm{dc}}\,\epsilon'_{\mathrm{ac}}$ 'stability space'. This knowledge can be obtained by solving (30) and (31), which, according to the unifying theory, yields universally stable regions, universally

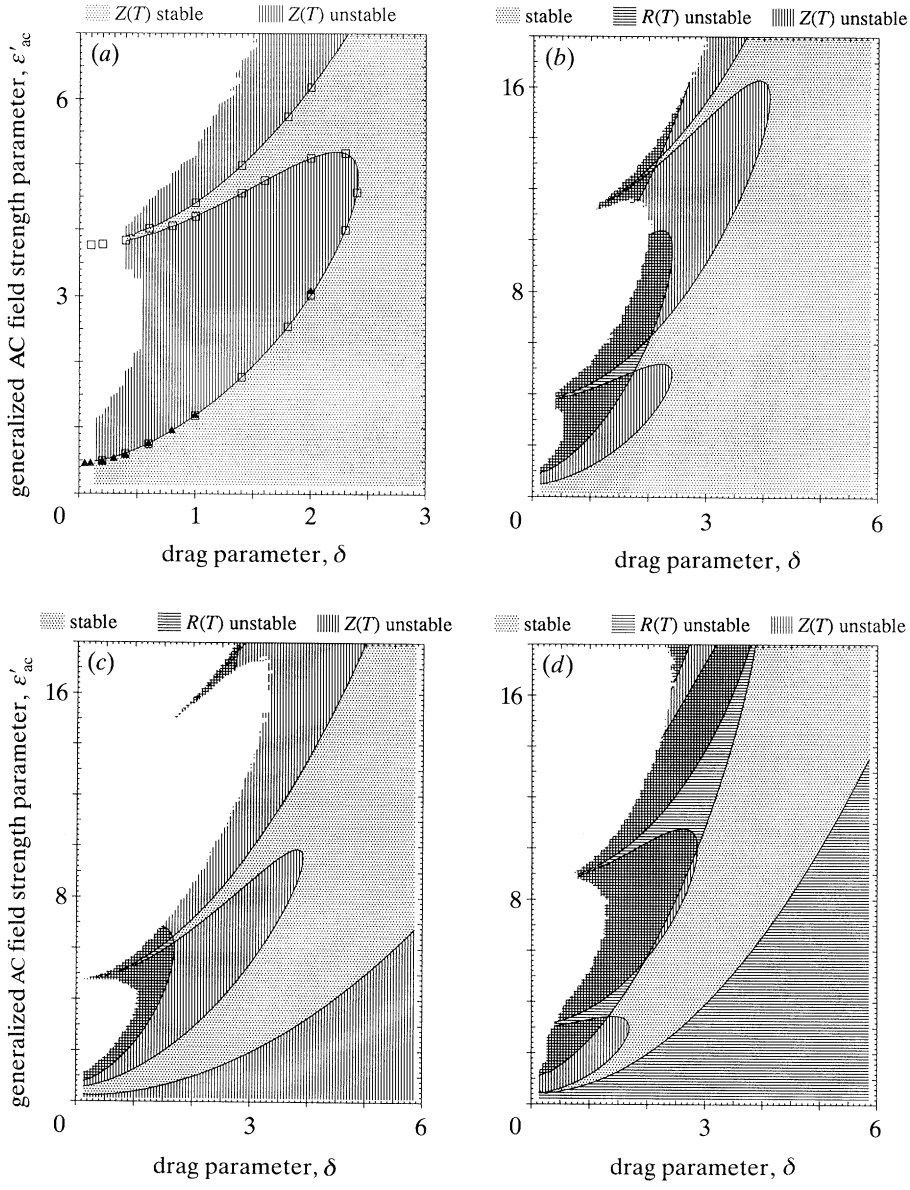

Figure 2. $\delta\epsilon'_{ac}$ stability diagrams. (*a*) Stability diagram for motion in the Z direction only for $\epsilon'_{dc} = 0$ obtained by numerical integration of (31). Symbols represent scaled results of Mathieu theory for the hyperboloidal (□) balance and of numerical integration for the triple-disc (▲) balance. Stability diagrams for (*b*) $\epsilon'_{dc}/\epsilon'_{ac} = 0$, (*c*) $\epsilon'_{dc}/\epsilon'_{ac} = 0.1$, and (*d*) $\epsilon'_{dc}/\epsilon'_{ac} = -0.1$, considering motion in both the R and Z directions, obtained by numerical integration of (30) and (31).

unstable regions and a universal boundary dividing them. As such, the stability boundary for any balance, when normalized with the value of C_1 appropriate to the shape, should coincide with the universal boundary.

Figure 2*a* (solid line) illustrates the universal stability boundary for motion in the Z direction obtained from the solution to (31) for the case $\epsilon'_{dc} = 0$. This curve was calculated numerically using methods described elsewhere (Hartung & Avedisian

1990). The curve defines the regions of stable operation for *any* balance shape once C_1 is known. Also shown in figure 2*a* (symbols) are previously reported theoretical results for two specific balance shapes, the hyperboloidal shape (Davis 1985) and the triple-disc shape (Ataman & Hanson 1969), normalized with the appropriate C_1 values. As expected, the stability boundaries for these balances coincide with the universal boundary.

We note that stability boundaries have conventionally been plotted only for Z, because stability regions for R can be obtained simply by scaling ϵ'_{ac} and ϵ'_{dc} by a factor of 2. However, a particle can be stably levitated only when its motion is stable in *all* directions. To underscore this fact, $\delta\epsilon'_{ac}$ stability diagrams for motion in both R and Z are shown for three different values of $\epsilon'_{dc}/\epsilon'_{ac}$ in figure 2*b–d*. The diagrams were obtained by numerical integration and stability analysis of (30) and (31). The changes in the Z instability regions produced by varying $\epsilon'_{dc}/\epsilon'_{ac}$ are in agreement with previous calculations (Davis 1985). However, our results are more complicated than we anticipated: figure 2 depicts the appearance of new instability regions near $\epsilon'_{ac} = 0$ and simultaneous shifts in the R instability regions as $\epsilon'_{dc}/\epsilon'_{ac}$ varies. These effects were not reported previously, although a new instability region for Z was also found by Frickel *et al.* (1978) in the case of $\epsilon'_{dc} = 0.1$, which is in qualitative agreement with figure 2*c*.

3. Field calculations

In the previous section, it was shown that the levitation and stability characteristics of a particular balance shape can be deduced solely from the levitation strength constant C_0 and the stabilization strength constant C_1, both of which are coefficients in the series expansion of the potential. In this section, the potential components will be calculated by solving (3) numerically and analytically for some balance shapes that have not been analysed previously. Values of C_0 and C_1 for these balance shapes will then be obtained from the potential components.

(*a*) *Numerical methods*

The POISSON group of programs (Winslow 1967; Warren *et al.* 1987) was used to obtain the potential and electric field numerically for several electrode configurations. It was necessary to impose an artificial boundary condition on part of the defined region, because the codes use a finite-difference mesh which cannot model infinitely large regions. Boundary segments connecting the ring electrode to the endcap electrodes were added to make the regions finite. In most cases, these segments were chosen to be approximately parallel to the electric field and a Neumann boundary condition was applied on them. Values of C_0 and C_1 were obtained from the numerically calculated potential components $V_+(R, Z)$ and $V_-(R, Z)$ by fitting these functions to the relations (8) and (9). More details on the numerical calculations are given in Hartung & Avedisian (1990).

(*b*) *Hyperboloidal configurations*

To test the numerical algorithm for solving the Laplace equation, a numerical solution for the known hyperboloidal shape was sought. The hyperboloidal configuration with $r_0/z_0 = \sqrt{2}$ was approximated using the region shown in figure 3*a*, *b*. The region differs from the ideal because the electric field is required to be perpendicular to a straight line segment connecting the ring electrode to an endcap electrode. The segment was chosen to be perpendicular to the asymptote $r/z = \sqrt{2}$

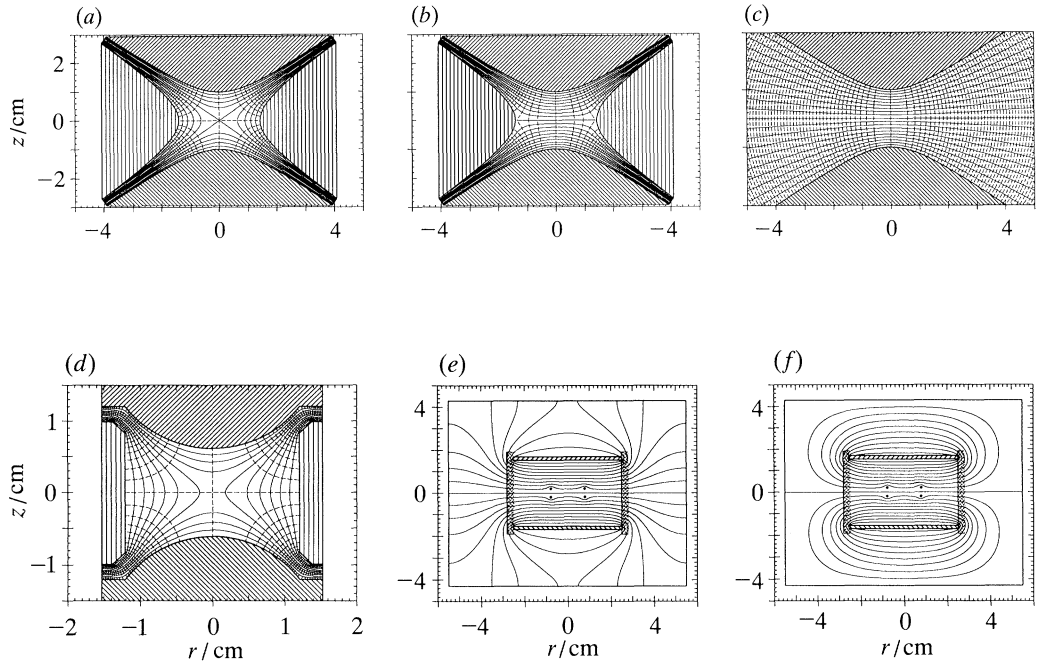

Figure 3. Equipotential lines (solid curves) and electric field lines (dashed curves) calculated for various balance shapes. (*a*) Even parity component, (*b*) odd parity component, and (*c*) analytically calculated approximation for the odd component (Davis 1985), for hyperboloidal electrodes with $r_0/z_0 = \sqrt{2}$. (*d*) Even parity component for the bihemispherical shape with a mesh size of $0.0164z_0$. Odd parity component with (*e*) a Neumann and (*f*) a Dirichlet boundary condition on the cylinder (equipotential lines only) for the double-ring/double-disc shape with a mesh size of $0.0130z_0$, and boundary conditions imposed on a cylinder a distance $1.753z_0$ away from the balance. All results except (*c*) are from numerical calculation.

and to intersect it at $R = R_{\mathrm{ma}}$. Since the ring electrode surface and the endcap electrode surfaces become parallel to the asymptotes at infinity, this boundary condition is correct in the limit $R_{\mathrm{ma}} \to \infty$. It is reasonable to expect that choosing R_{ma} large enough should yield a solution identical to the analytical solution to the accuracy of the numerical results. The difference between the numerical and analytic solutions was found to be a strong function of the mesh size and a weak function of R_{ma} for $R_{\mathrm{ma}} \geqslant 2$. For the range of values of R_{ma} and mesh sizes investigated, $R_{\mathrm{ma}} = 4$ and a nominal mesh spacing of $0.02z_0$ yielded the optimum numerical solution.

Figure 3*a*, *b* shows equipotential lines (on which v is constant) and electric field lines (tangent to $\boldsymbol{E}$) near the origin for the two components of this solution. The electric field lines plotted in figure 3 are spaced so that the electric flux through a surface of revolution connecting two adjacent lines is a constant; the field lines are plotted by finding equipotentials of an 'electric vector potential'. The numerical result for the even component in figure 3*a* agrees very well with the analytic results of Wuerker *et al.* (1959). For the odd component, the only known analytic solution (figure 3*c*) is approximate (it is correct only in the limit $r_0/z_0 \to \infty$), and the numerical result which accounts for the presence of the ring electrode (figure 3*b*) is noticeably different from it. The numerical result suggests that the ring electrode affects the odd-parity field components significantly.

Calculated values of C_0 were found to have a very weak dependence on balance

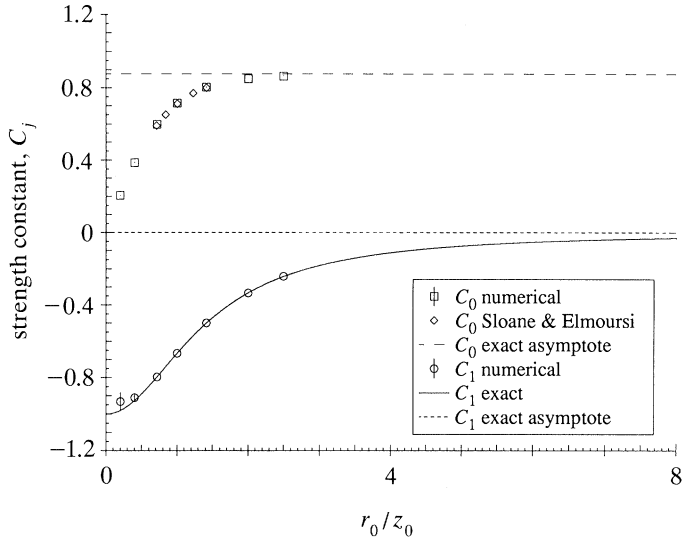

Figure 4. Dependence of C_0 and C_1 on the balance design parameter r_0/z_0 for the hyperboloidal balance with $R_{ma} = 4$. The solid curve represents the exact analytic solution for C_1; the dashed lines represent the exact values in the limit $r_0/z_0 \to \infty$. Symbols refer to numerical results. Bars are based on estimated lower bounds on the error in the values due to the numerical calculation. In many cases, the estimated error is too small to be visible.

radius R_{ma} for $R_{ma} \geqslant 1.5$, which suggests that C_0 can be predicted accurately for the ideal shape ($R_{ma} \to \infty$). Figure 4 compares our results for C_0 as a function of r_0/z_0 with previously reported values (Sloane & Elmoursi 1987). The value for $r_0/z_0 \to \infty$ is an analytic result (Davis 1985). The values from different sources are reasonably consistent with one another. Calculated values of C_1 did not show any statistically significant dependence on R_{ma} for $R_{ma} \geqslant 2$. Our calculated values of C_1 as a function of r_0/z_0 are also compared with the theoretical values in figure 4. For $r_0/z_0 > \frac{1}{2}$, the numerical values agree very well with the exact values; for $r_0/z_0 > \frac{1}{2}$, they deviate from the exact result, but by an amount about equal to the estimated error. This indicates that the numerical technique is capable of producing accurate results, but not always precise ones.

(*c*) *Other configurations*

A bihemispherical electrode configuration (figure 1*g*) was analysed numerically. This balance shape consists of two hemispheres and a cylinder, connected by flanges with insulating rings; dimensions were obtained from a scale drawing (Richardson & Spann 1984). For the numerical solution, the shape was simplified by omitting the insulating rings and the outer step in the flanges where the rings were placed. The region was made finite by imposing the condition that the electric field be vertical at the outer radius of the flanges. The calculated field components, one of which is shown in figure 3*d*, are qualitatively similar to the hyperboloidal results except near the flanges. The field components calculated for a similar shape (figure 1*f*) deviated more from the fields in the hyperboloidal shape.

The 'double-ring/double-disc' configuration (figure 1*e*) was also examined numerically. This balance consists of two flat disc endcap electrodes, held in place by a plexiglass tube, and two metal rings of circular cross-section connected to a conducting support which serve as the ring electrode. Dimensions given by Ward

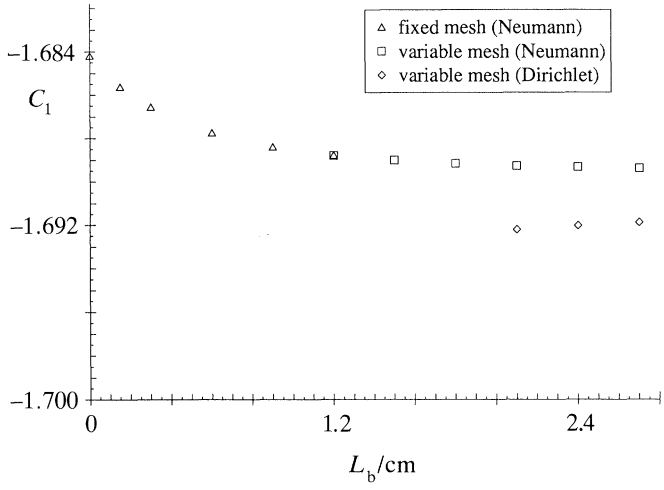

Figure 5. Dependence of C_1 on the distance to the bounding cylinder for the double-ring/double-disc balance for both of the possible boundary conditions on the cylinder.

(1989) were used; the thickness of the endcap electrodes and the thickness of the plexiglass tube were taken to be 0.5 mm and 3 mm, respectively, relative to the balance characteristic dimension $z_0 = 15.4$ mm. The dielectric constant of the plexiglass tube was set to 3, and it was assumed not to extend beyond the edge of the endcap electrodes. The effect of the support piece for the rings was neglected.

In contrast to the other balances examined in this study, the double-ring/double-disc shape has open boundaries over a large area. To approximate the ideal case of a region of infinite size with a boundary condition imposed at infinity, the balance was surrounded by a cylinder a distance L_b away from the endcap electrodes and from the plexiglass tube. A Neumann boundary condition was imposed on the surface of the cylinder. The result for one component, with $L_b = 27$ mm, is shown in figure 3*e*. Figure 3*e* suggests that the presence of the rings affects the levitating field significantly. A Dirichlet boundary condition was also tried to gauge the perturbation due to the presence of the cylinder, as in the limit $L_b \to \infty$, the solution should be independent of the imposed boundary condition. The result is shown in figure 3*f*. Changing the boundary condition significantly influences the fields near the cylinder, but does not strongly affect the fields inside the balance.

Figure 5 shows C_1 as a function of the distance L_b to the bounding cylinder for both boundary conditions on the bounding cylinder. The calculated values for the two different boundary conditions are evidently converging to a common value as $L_b \to \infty$. Figure 5 suggests that reasonably accurate results can be obtained without an excessively large value of L_b (note that differences in C_1 are less than 0.2% for $L_b > 20$ mm). Results for C_0 (not shown) are similar.

Based on the agreement between the results with different boundary conditions, one would not expect the field to depend strongly on the thickness of the endcap electrodes or the amount by which the plexiglass tube extends above them. The same cannot be said of the dielectric constant and thickness of the plexiglass tube, however, so their influence on the calculated values of C_0 and C_1 was estimated. Changing the dielectric constant from 3 to 3.25 decreased the calculated C_0 by 0.01%, while $|C_1|$ increased by 0.03%; changing the thickness of the dielectric from 3 mm to 3.5 mm increased the calculated C_0 by 0.1% and decreased $|C_1|$ by 0.04%.

Numerically calculated values of C_0, C_1, and several higher coefficients are given in table 2 for the double-ring/double-disc, bihemispherical and hyperboloidal balances. The error estimates listed in table 2 are based on the error (i) from the fit of the potential components, (ii) due to the non-zero mesh spacing, and (iii) due to the finite region size. The lower error bounds listed in table 2 are based on (i) only.

(*d*) *An analytic solution for the pillbox shape*

A particularly simple electrode configuration, for which the fields can be found analytically, is shown in figure 1*i*. For this 'pillbox' shape, the ring electrode is a cylinder and the endcap electrodes are flat discs. The endcap electrodes touch the ring electrode in the ideal case, making the potential discontinuous; as with the spherical void shape shown in figure 1*h*, the electrodes must be separated by some amount to make the balance practical.

To find the potential for the pillbox shape, it is advantageous to use cylindrical coordinates (r, z, φ). With axial symmetry, separation of variables yields a general solution in terms of Bessel functions. Under the restriction that $v(0,0)$ be finite, the solution takes the form

$$v(r,z) = \sum_k [\alpha_k \sinh(kz) + \beta_k \cosh(kz)] J_0(kr), \tag{32}$$

where the values of k to be summed over are determined by the boundary conditions. The potential can be resolved into its dimensionless odd parity and even parity components to yield expressions for $V_+(R,Z)$ and $V_-(R,Z)$. The boundary conditions $V_+ = 1$ and $V_- = 0$ for $R = r_0/z_0$, require that $J_0(kr_0) = 0$ for all non-zero k, which gives

$$V_+(R,Z) = 1 + \sum_{j=1}^{\infty} B_j \cosh\left(x_j \frac{z_0}{r_0} Z\right) J_0\left(x_j \frac{z_0}{r_0} R\right), \tag{33}$$

$$V_-(R,Z) = \sum_{j=1}^{\infty} A_j \sinh\left(x_j \frac{z_0}{r_0} Z\right) J_0\left(x_j \frac{z_0}{r_0} R\right). \tag{34}$$

The boundary conditions $V_+ = 0$ and $V_- = 1$ for $Z = 1$ can be satisfied via the proper choice of the coefficients A_j and B_j, with the result

$$V_+(R,Z) = 1 - 2\sum_{j=1}^{\infty} \frac{\cosh(x_j(z_0/r_0)Z)\, J_0(x_j(z_0/r_0)R)}{x_j \cosh(x_j z_0/r_0)\, J_1(x_j)}, \tag{35}$$

$$V_-(R,Z) = 2\sum_{j=1}^{\infty} \frac{\sinh(x_j(z_0/r_0)Z)\, J_0(x_j(z_0/r_0)R)}{x_j \sinh(x_j z_0/r_0)\, J_1(x_j)}. \tag{36}$$

Equations (35) and (36) represent a full solution for the fields in the pillbox balance. The potential components can be expanded in terms of the harmonic functions of (8) and (9), which gives

$$C_0 = 2\frac{z_0}{r_0} \sum_{j=1}^{\infty} \frac{1}{\sinh(x_j z_0/r_0)\, J_1(x_j)}, \tag{37}$$

$$C_1 = -\left(\frac{z_0}{r_0}\right)^2 \sum_{j=1}^{\infty} \frac{x_j}{\cosh(x_j z_0/r_0)\, J_1(x_j)}. \tag{38}$$

The above sums converge fairly rapidly except when $r_0/z_0 \gg 1$.

The first few terms in (37) and (38) were evaluated for r_0/z_0 between 0 and 8. The first 30 terms were found to give satisfactory accuracy in that range. The corresponding values of C_0 and C_1 are shown in figure 6. The dependence on r_0/z_0 for

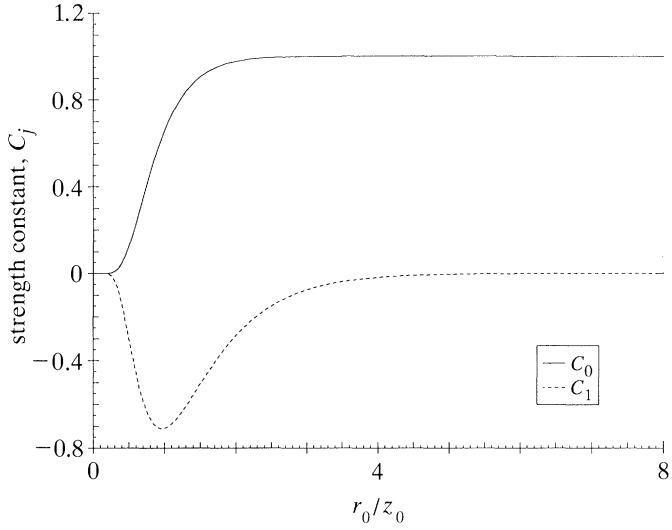

Figure 6. Dependence of C_0 and C_1 on the balance design parameter r_0/z_0 for the pillbox shape, based on the first 30 terms in the series expressions (37) and (38).

Table 2. *Numerically calculated series coefficients*

(The symbol $\geqslant$ denotes lower bounds on the error.)

balance shape	C_0	C_1	C_2
hyperboloidal	0.802787	−0.499993	0.19641
$r_0/z_0 = \sqrt{2}$ (figure 1*a*)	±0.000091	±0.000023	± ⩾ 0.00011
hyperboloidal	0.59747	−0.79588	0.5237
$r_0/z_0 = \frac{5}{7}$	± ⩾ 0.00052	± ⩾ 0.00082	± ⩾ 0.0024
spheres/cylinder	0.508076	−0.5425379	0.398871
(figure 1*f*)	± ⩾ 0.000012	± ⩾ 0.0000001	± ⩾ 0.000029
bihemispherical	0.834611	−0.3837194	0.162830
(figure 1*g*)	± ⩾ 0.000033	± ⩾ 0.0000002	± ⩾ 0.000078
double-ring/double-disc	0.8156	−1.690	0.8833
(figure 1*e*)	±0.0067	±0.029	± ⩾ 0.0011

balance shape	C_3	C_4	C_5
hyperboloidal	$-4.91\ (10^{-6})$	$-6.32\ (10^{-3})$	$-0.2080\ (10^{-6})$
$r_0/z_0 = \sqrt{2}$ (figure 1*a*)	$\pm \geqslant 0.25\ (10^{-6})$	$\pm \geqslant 0.18\ (10^{-3})$	$\pm \geqslant 0.0039\ (10^{-6})$
hyperboloidal	$-2.9\ (10^{-3})$	-0.1942	$8.3\ (10^{-3})$
$r_0/z_0 = \frac{5}{7}$	$\pm \geqslant 2.9\ (10^{-3})$	$\pm \geqslant 0.0074$	$\pm \geqslant 8.3\ (10^{-3})$
spheres/cylinder	−0.2067098	0.088090	−0.02496145
(figure 1*f*)	± ⩾ 0.0000002	± ⩾ 0.000045	± ⩾ 0.00000023
bihemispherical	$-7.894039\ (10^{-3})$	$1.93\ (10^{-3})$	$7.08263\ (10^{-3})$
(figure 1*g*)	$\pm \geqslant 0.000016\ (10^{-3})$	$\pm \geqslant 0.12\ (10^{-3})$	$\pm \geqslant 0.00013\ (10^{-3})$
double-ring/double-disc	2.1026	−2.9401	1.469
(figure 1*e*)	± ⩾ 0.0034	± ⩾ 0.0079	± ⩾ 0.022

the pillbox shape is qualitatively similar to the results one obtains for the spherical void balance (figure 1*h*) using the expressions for C_0 and C_1 given in table 1 and associating r_0/z_0 with $\tan\theta_m$.

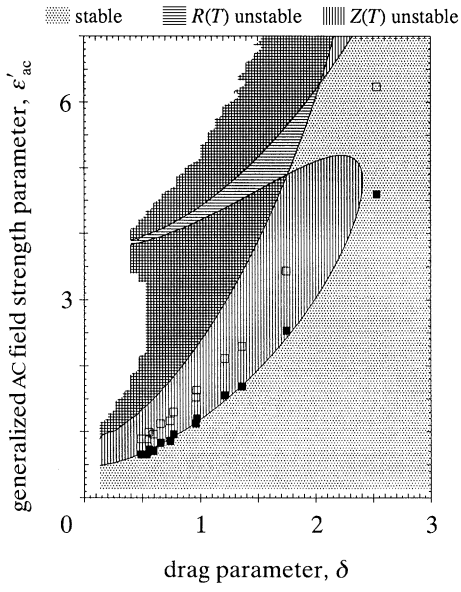

Figure 7. Comparison of $\delta\epsilon'_{ac}$ stability predictions for $v_{dc} = 0$ from numerical integration of (30) and (31) with experimental stability results for the double-ring/double disc balance. Symbols represent experimentally measured points along the stability boundaries scaled using the numerically calculated value of C_1/C_0 (□) and an empirical C_1/C_0 value (■) chosen to minimize the difference between the theoretical curve and the experimental data.

(*e*) *Comparison with experimental results*

Several methods can be used to obtain values of C_0 and C_1 experimentally. One standard balance calibration method is the *Sprungpunkt* technique, in which a particle is levitated at the null point and the alternating potential (and/or frequency) is adjusted to find the instability boundary. The levitating potential gives qC_0/m via (22), which is used along with v_{ac} and Ω to obtain $C_0\epsilon_{ac}$. Values of $C_0\epsilon_{ac} = -\frac{1}{2}(C_1/C_0)\epsilon'_{ac}$ as a function of δ can thereby be measured along the instability boundary. Because the $C_0\epsilon_{ac}$ values differ from ϵ'_{ac} by a factor of $-\frac{1}{2}C_1/C_0$ only, an experimental value of C_1/C_0 can be obtained by scaling the experimental $C_0\epsilon_{ac}$ against δ curve to fit the theoretical instability boundaries in the $\delta\epsilon'_{ac}$ plane. Stability data obtained using this method for the double-ring/double-disc balance (Ward 1989, figure 2.4) are compared with a numerically calculated stability diagram in figure 7, using (i) the numerically calculated value of C_1/C_0 and (ii) an experimental C_1/C_0 chosen as described above. The two values of C_1/C_0 produce significantly different results, but the experimental value yields scaled data that reproduce the theoretical curve reasonably well.

Values of C_0 and C_1 obtained experimentally for various balance shapes are listed in table 3. The result in table 3 for the double-ring/double-disc shape is based on the above analysis. In all but three cases, only the ratio of C_0 to C_1 was measured. A theoretical value for one of the two parameters was often used to calculate the other. Theoretical values from tables 1 and 2 are also listed in table 3 where possible.

The agreement between the experimental and theoretical values in table 3 ranges from very good to very poor. The lack of agreement between different experimental results for the same balance shape suggests that either the theory is inadequate or the shapes used experimentally are significantly different from those used to predict

Table 3. *Experimental values of coefficients C_0 and C_1*

hyperboloidal balances with asymptote slope = $\sqrt{2}$ and $r_0/z_0 = \sqrt{2}$ (figure 1*a*)

refer to		C_0 (measured)		theoretical C_0
Philip (1981), Philip *et al.* (1983)	—	0.805 ± 0.015[a]	—	0.803
Philip (1981)	—	0.707 ± 0.049[b]	—	
	C_1/C_0 (measured)	C_0 (inferred)	C_1 (assumed)	theoretical C_1/C_0
Davis (1985)	-1.06 ± 0.12	0.471 ± 0.054	$-\frac{1}{2}$	-0.623
Davis (1985), Davis *et al.* (1988)	-0.54	0.92	$-\frac{1}{2}$	-0.623
Davis *et al.* (1988)	-0.427	1.17	$-\frac{1}{2}$	-0.623
Sageev *et al.* (1986)	-0.70	0.71	$-\frac{1}{2}$	-0.623

hyperboloidal balances with asymptote slope = $\sqrt{2}$ and r_0/z_0 variable

refer to	r_0/z_0	C_1/C_0 (measured)	C_0 (inferred)	C_1 (assumed)	theoretical C_1/C_0
Ward *et al.* (1989), Ward (1989)	*ca.* $\sqrt{2}$ (1.33)	-0.588 ± 0.012	0.85 ± 0.017	$-\frac{1}{2}$	*ca.* -0.623
Ward (1989)	*ca.* $\sqrt{2}$ (1.54)	-0.455 ± 0.014	1.10 ± 0.034	$-\frac{1}{2}$	*ca.* -0.623
Frickel *et al.* (1978)	$\frac{5}{7}$	-1.286 ± 0.007	0.620 ± 0.004[c]	$-\frac{98}{123}$	-1.334

other balance shapes

balance shape	figure	refer to	C_1/C_0 (measured)	C_0 (assumed)	C_1 (inferred)	theoretical C_1/C_0
triple-disc $r_0/z_0 = \frac{4}{3}$	1*b*	Ataman & Hanson (1969)	-0.332 ± 0.011	1	-0.332 ± 0.011[d]	-0.368
		Schweizer & Hanson (1971)	-0.3634 ± 0.053	1	-0.3634 ± 0.053[e]	-0.368
bihemispherical	1*g*	Richardson & Spann (1984)	-0.35[f]	—	—	-0.46
		Richardson *et al.* (1986)				
double-ring/double-disc	1*e*	Ward (1989)	-1.53 ± 0.02[g]	—	—	-2.1
				C_0 (measured)		
double-ring/cylinder, $z_0 \equiv z_R$	1*f*	Berg *et al.* (1970)		0.776[h]		

[a] Calculated from data in Table 4.1; same data appear in Table I of Philip *et al.* (1983). [b] Calculated from data in Table 4.1. [c] From the result $C_{dc} = 17.1\ m^{-1} \pm 0.1\ m^{-1}$. [d] From the result $C = 1.18 \pm 0.04$. [e] From the result $C = 1.292 \pm 0.019$. [f] From the result $C = 2250\ s^{-2}$, using a scale drawing (Richardson & Spann 1984), and making assumptions. [g] Calculated from data in figure 2.4. [h] From the result $k_{dc} = 3.52\ (10^3)$; the shape is qualitatively similar to figure 1*f*.

the C_js. The shapes of actual balances are in fact often quite a bit different from the ideal shapes they are based on. For example, two hyperboloidal balances listed in table 3 both have a 'nominal' r_0/z_0 of $\sqrt{2}$, but the actual balances have $r_0/z_0 = 1.33$ and 1.54. Figure 4 suggests that perturbations in r_0/z_0 of that order can change C_1/C_0 by about 10%. Another example of deviation from the ideal shape is the presence of holes in the endcap electrodes. In one balance, a hole of a radius $\frac{107}{240}z_0$ was present in the upper endcap electrode (Ward 1989). Numerical calculations with such a hole in both endcap electrodes predict a 2% change in C_1/C_0, with C_0 decreasing by 5% and $|C_1|$ decreasing by 7%. These results suggest that the differences between the experimental and theoretical values might be accounted for solely by differences in balance shape.

4. Optimum balance shapes

A number of balance shapes that have been used experimentally are shown in figure 1. Each shape produces a unique electric field environment for particle levitation and stabilization which depends on the size and shape of the electrodes. It is natural to expect that there is a 'best' or 'optimum' balance shape.

If there are no limits to the levitating and stabilizing fields that a balance can operate with, any balance can stably levitate a particle with any mass m and any non-zero charge q, so that any two balances can in principle levitate a particle with the same degree of stability via the proper choice of the levitating and stabilizing potentials for each. Thus, in theory, no balance is better at levitation or stabilization than another. In practice, however, there are limits on the fields that can be achieved in real balances. There are limits on (i) the potentials that can be applied to the balance electrodes (since power supplies only generate finite potentials), and (ii) the surface electric fields that can be supported by the balance electrodes (above which phenomena such as arcing or field emission occur).

A balance subjected to these limits cannot suspend a charged particle of arbitrary m and q. Rather, the limits on the allowable surface fields and potentials produce an upper bound on m/q, above which the particle can no longer be held in the balance. We assume that the better of two balances is the one which can suspend the particle with the largest possible m/q when both balances are subject to the same limits on the applied potentials or the surface fields. This is by no means the only optimization criterion one could envisage, nor is it an appropriate criterion for all applications. Other considerations include sensitivity to small perturbations in the applied potentials or electrode shape, difficulty of particle injection, etc. A criterion based on maximizing m/q was chosen because of its relevance to applications in which a large particle mass or a small particle charge (needed for electron stepping measurements, for instance) are desired. This criterion is particularly germane for combustion studies in which large droplets of liquid fuels with small charges (a liquid particle's charge is limited by Rayleigh instability) are needed.

(*a*) *Optimization with limited potentials*

When the available potentials limit the performance of a balance, the applied stabilizing and levitating potentials can be fixed while comparing different balance shapes. For stabilization, the stability space parameters ϵ'_{ac}, ϵ'_{dc}, and δ can also be fixed. From the definition of ϵ'_{ac}, we have

$$m/q = -2C_1 v_{\mathrm{ac}}/\epsilon'_{\mathrm{ac}} z_0^2 \Omega^2. \tag{39}$$

Thus, for given values of the potential (v_{ac}), stability parameter (ϵ'_{ac}), frequency (Ω), and balance size (z_0), the largest m/q is obtained with the largest value of $|C_1|$: the larger $|C_1|$, the better the balance is for stabilization (the same conclusion follows from the definition of ϵ'_{dc}, if a static potential is also applied to the ring). Similarly, (22) shows that the larger $|C_0|$, the better the balance is for levitation, when v_{end} and z_0 are fixed.

The presence of the balance size parameter z_0 in (22) and (39) shows that the size of the balance influences its performance: a balance's stabilization and levitation abilities improve as its dimensions (via z_0) are scaled down and worsen as its dimensions are scaled up. Consequently, it is important to factor out the influence of balance size when comparing performance. This can be done by choosing the same value of z_0 for all the balances. However, the way in which z_0 is defined for each shape then becomes significant; any balance shape can be made to appear superior with a proper definition of z_0. To avoid this difficulty, we will require that the particle be surrounded by a volume of empty space of some *given* shape. The size of this volume will be used to obtain a universal length scale to replace z_0 in the calculation of C_0 and C_1 for all balances. Two balances will be taken to have the same size when they are built around empty volumes of the same size and shape, i.e. when they have the same characteristic length z_c. We believe that this provides the only meaningful basis for comparing different shapes. The parameters C_0 and C_1 are now redefined to incorporate the universal length scale instead of z_0:

$$C_0 \rightarrow D_0 \equiv (z_c/z_0)\, C_0, \tag{40}$$

$$C_1 \rightarrow D_1 \equiv (z_c/z_0)^2\, C_1. \tag{41}$$

Therefore, the larger $|D_0|$ and $|D_1|$ are, the better the balance. The best balance is the one for which $|D_0|$ and $|D_1|$ are maximized.

As an example, we choose a spherical excluded volume for the comparison constraint. The sphere's radius r_{s0} is a suitable choice for the characteristic length z_c. The relation between z_c (i.e. r_{s0}) and z_0 is determined by finding the largest sphere that can be inscribed inside the balance electrodes for each shape. A plot of theoretical values of D_1 against D_0 for several balance shapes in the spherical excluded volume case, based on both exact and numerical calculations, is shown in figure 8. Unique balance shapes are represented by points in figure 8; shapes with a variable parameter are represented by curves. The discontinuity in the slope of the curve for the hyperboloidal, triple-disc and pillbox balances corresponds to the discontinuity in the definition of D_0 and D_1 at $r_0/z_0 = 1$.

The spherical void electrodynamic levitator (the SVEL balance, figure 1*h*) is clearly the best balance of those shown in figure 8, since it has the maximum $|D_1|$ for any given D_0 and the maximum $|D_0|$ for any given D_1. For the SVEL shape, we see from table 1 (using the fact that $D_j = C_j$ for the SVEL shape in this case) that $|D_0|$ is maximized when $\theta_m = 90°$, whereas $|D_1|$ is maximized when $\theta_m = \arccos(1/\sqrt{3}) = 54.74° \equiv \theta_1$. Thus, of the shapes considered, the best balance for levitation is the SVEL balance with $\theta_m = 90°$, while the best balance for stability is also the SVEL balance, but with $\theta_m = \theta_1$. The latter θ_m value was used by Arnold & Folan (1987). At this point, there is no balance in which both levitation and stability are optimized simultaneously (see §5, however).

In the above example, the 'best' balance shape was found to be the shape in which the electrodes completely enclose the excluded volume chosen as a constraint (i.e. an empty sphere produces a spherical void shape). This suggests that an optimum

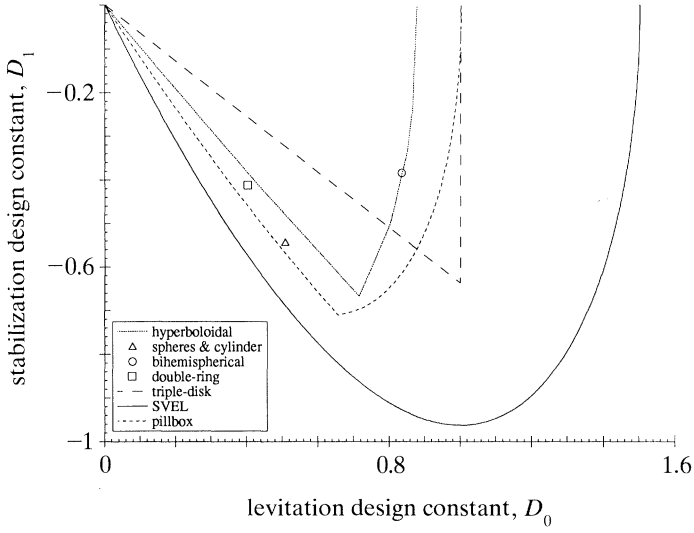

Figure 8. An electrodynamic balance design diagram showing the relationship between the design coefficients D_0 and D_1 for different balance shapes under the constraint of a spherical excluded volume. All values are theoretical. The curves for the hyperboloidal, triple-disc, and pillbox balance correspond to varying r_0/z_0; the curve for the SVEL balance corresponds to varying θ_m. Results for the triple-disc shape are obtained from the approximate analytic result (table 1).

balance shape does not emerge independently of the choice of excluded volume. We are led to the hypothesis that any balance shape can be elevated to the position of optimum balance shape simply by selecting the shape of the excluded volume to coincide with the region outside the electrodes in the chosen shape. This hypothesis is proved in Appendix B. Consequently, *no 'natural' balance shape emerges independently of the chosen excluded volume, and no balance shape is intrinsically better than another in the potential-limited case.* There is thus no intrinsic advantage to the hyperboloidal shape, the triple-disc shape, the SVEL shape, or any other.

An excluded volume must be defined *a priori* in order to factor out the influence of the relative size of different balances in the performance comparison. If the shape of the excluded volume is left as a parameter to be determined as part of the optimization, $|D_0|$ and $|D_1|$ can be made arbitrarily large with an excluded volume in which the distance between the particle and one of the electrode surfaces goes to zero, producing a highly optimal but completely impractical balance shape. Some excluded volume shape must be chosen, and the optimum balances that emerge will incorporate that choice.

The lack of a unique optimum shape does not mean that all balances are just as good or just as bad for a particular application. Practical concerns can be used to dictate a choice for the excluded volume shape and hence for the electrode contour. For some applications, the distance to the electrodes in the z direction may be more important than the distance to the electrodes in the r direction, because the gravitational force in the z direction can produce vertical oscillations of the particle when the levitating field is not adjusted to balance it exactly. In such a situation, it would be more appropriate to choose a cylindrical or ellipsoidal shape rather than a spherical shape.

Once an appropriate shape is chosen, the electrode configuration must still be determined. It is shown in Appendix B that, for any given excluded volume shape,

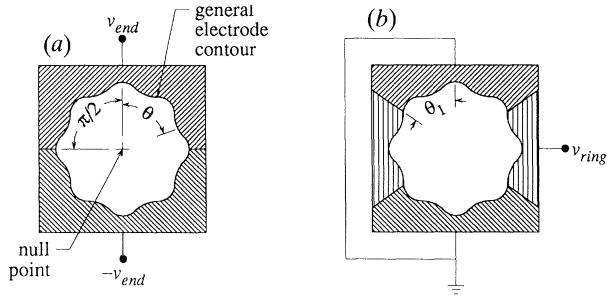

Figure 9. The electrode configurations for (*a*) optimizing levitation and (*b*) optimizing stability for a general excluded volume shape (unshaded region).

there are two optimum electrode configurations; one for optimum levitation and the other for optimum stability. In terms of the polar angle θ (figure 9*a*), it is shown in Appendix B that the balance is optimized for levitation by

(i) applying the positive levitating potential (v_{end}) to surfaces between $\theta = 0$ and $\theta = \frac{1}{2}\pi$ and

(ii) applying the negative levitating potential ($-v_{\text{end}}$) to surfaces between $\theta = \frac{1}{2}\pi$ and $\theta = \pi$.

On the other hand, the balance is optimized for stability by

(iii) applying the stabilizing ring potential (v_{ring}) to surfaces between $\theta = \theta_1$ and $\theta = \pi - \theta_1$ and

(iv) grounding the rest of the surfaces.

The two configurations are illustrated schematically in figure 9 for a 'general' excluded volume shape. It should be noted that the optimum electrode configuration for levitation provides no stability, since there is no ring electrode. The optimum configuration for stability can provide levitation if we apply a potential across the grounded surfaces (i.e. apply v_{end} to surfaces between $\theta = 0$ and $\theta = \theta_1$ and apply $-v_{\text{end}}$ to surfaces between $\theta = \pi - \theta_1$ and $\theta = \pi$), but the balance will be less than optimal for levitation.

(*b*) *Optimization with limited surface fields*

In practical applications, the operation of a balance can be limited by high surface electric fields rather than by the available potentials. For example, arcing across the electrodes may occur before the applied potentials reach their maximum values. In that event, the surface fields limit the performance of a balance and the available potentials do not.

In the surface field-limited case, we still want to maximize $|C_0|$ and $|C_1|$ to optimize levitation and stabilization, respectively, but with the maximum surface fields fixed, rather than with fixed potentials. For levitation, we see from (12) that maximizing $|C_0|$ is equivalent to maximizing the dimensionless electric field at the null point ($R = Z = 0$). We can optimize for levitation by maximizing the ratio of the electric field at the null point to the maximum surface electric field (in magnitude). This ratio does not depend on the size of the balance, so no characteristic lengths are needed. For an electrostatic field, the maximum value of this ratio is 1. A field ratio of 1 is obtained only with a spatially uniform field, which is produced by infinite parallel plates. The ideal triple-disc shape in which $r_{\text{D}} \to \infty$ and $h \to 0$ (figure 1*b*) also produces a uniform levitating field, so *the ideal triple-disc shape is the optimum shape for levitation in the surface field-limited case.*

The stabilization analysis is a bit more complicated, and we have not found an optimum shape for stability. We note, however, that the balance size becomes important again in the optimization of $|C_1|$ at a fixed maximum surface field, which leads us to hypothesize that there may not be a unique optimum shape for stability. We also note that optimum shapes for the potential-limited situation and optimum shapes for the surface field-limited situation represent opposite extremes: for any of the optimum shapes of §4*a*, the electrodes always touch one another, so that the surface fields are in theory infinite. Slight modifications to the electrode configuration will always be required for shapes optimized for potential-limited scenarios. One should be able to estimate rather easily how close the electrodes can be safely placed in a given design.

5. Performance enhancement via function sharing

Although no unique optimum balance shape exists in the potential-limited case, it is possible to optimize the performance of a balance whose shape is given. In §4*a*, it was shown that, for a given excluded volume, and the *de facto* optimum shape in which the electrodes completely enclose the excluded volume, there are two optimum electrode configurations in the potential-limited case, one in which levitation is optimized (with no stability) and one in which stability is optimized (with non-optimal levitation). A simple refinement to the electrode configuration is now proposed to allow levitation and stabilization to be optimized simultaneously in a potential-limited situation.

In the traditional electrodynamic balance, the applied levitating and stabilizing potentials are spatially distinct: the odd parity levitating field is produced by applying static potentials of opposite sign to the upper and lower endcap electrodes, and the even parity stabilizing field is produced by applying an AC potential (with a DC component also, if desired) to the ring electrode. The fact that the two field components have opposite parity, however, means that they can always be resolved. One can hence start with a balance that has been optimized for stability, divide the ring electrode into two symmetric halves, and use these halves as both the ring electrode and part of the two endcap electrodes simultaneously. The balance will then be optimized for both levitation and stabilization. In terms of the polar angle θ (figure 9), this means applying

(i) the positive levitating potential (v_{end}) to surfaces between $\theta = 0$ and $\theta = \frac{1}{2}\pi$,

(ii) the negative levitating potential ($-v_{\text{end}}$) to surfaces between $\theta = \frac{1}{2}\pi$ and $\theta = \pi$, and

(iii) the stabilizing ring potential (v_{ring}) in series with the levitating potential between $\theta = \theta_1$ and $\theta = \pi - \theta_1$.

The two ring electrode halves thus share the function of both ring electrode and endcap electrode; we call this method of improving performance 'function sharing'.

The above recipe optimizes the performance for any given balance shape with axial symmetry. As an example, figure 10 shows the arrangement that is obtained with the SVEL balance (figure 1*h*). For the configuration shown in figure 10, D_0 is equal to the SVEL value with $\theta_m = 90°$ (optimum for levitation) and D_1 is equal to the SVEL value with $\theta_m = \theta_1$ (optimum for stability). This electrode configuration, which we call FSSVEL (function sharing spherical void electrodynamic levitator), optimizes the spherical void shape for levitation and stabilization simultaneously. Function sharing can be applied to the pillbox shape (figure 1*i*), by redistributing the applied

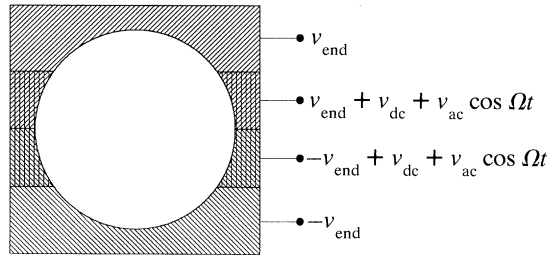

Figure 10. Electrode configuration for a 'function sharing spherical void' balance. It should be noted that the way in which the electrodes are joined together outside the void does not affect the fields inside the balance; connecting the electrodes via a 'cone' joint as in figure 9 produces the same effect as the 'flange' joint shown here.

potentials in a similar manner. When $r_0/z_0 = \sqrt{2}$, the stabilizing potential is applied to the cylinder only and not to the discs, yielding a particularly simple electrode configuration.

Function sharing optimizes the performance of a given balance shape only when the electrodes enclose the desired excluded volume. Function sharing can potentially improve the performance of any balance, however. The levitation ability of the double-ring/double-disc balance, for example, could be enhanced by applying the levitating potential across the two rings as well as across the endcap electrodes. It should be noted that function sharing is already used with the double-ring balance (figure 1*d*), allowing the number of electrodes to be reduced to two.

The authors thank H. Stokes and T. Barts of the Accelerator Code Group at Los Alamos National Laboratory for providing a copy of the POISSON programs and sharing their expertise with these codes, R. Helmke and the Cornell Laboratory of Nuclear Studies for granting us the use of their computer facilities, and B. Benedict for assistance in preparing this document. Conversations with Professor E. J. Davis of the University of Washington, Dr T. L. Ward of the University of New Mexico and Professor S. Arnold of the Polytechnic University (New York) are also gratefully acknowledged. This work was supported by the National Science Foundation under grant no. CBT-8451075.

Appendix A

We assumed in §2*a* that $\rho = 0$ everywhere except on the electrode surfaces, thus neglecting the charge of the suspended particle. We now examine the validity of this assumption by estimating the effect of a single charged particle on the analysis.

With a charged particle inside the balance, we must solve (1), rather than (3), with specified potentials on the electrode surfaces. We can express the solution $v(\boldsymbol{r})$ to (1) as the sum of two component potentials, $v_0(\boldsymbol{r})$ and $v_i(\boldsymbol{r})$, such that $v_0(\boldsymbol{r})$ satisfies (3) with the desired boundary conditions on the electrode surfaces and $v_i(\boldsymbol{r})$ satisfies (1) with the boundary condition $v_i = 0$ on all electrode surfaces. Because (1) is linear, $v(\boldsymbol{r}) = v_0(\boldsymbol{r}) + v_i(\boldsymbol{r})$ is the exact potential which accounts for both the potentials applied to the electrodes and the presence of the charged particle. The component $v_0(\boldsymbol{r})$ is then the charge-free potential discussed previously, while $v_i(\boldsymbol{r})$ is an induced potential due to the presence of the charge. Finding $v_i(\boldsymbol{r})$ for an arbitrary balance shape is a non-trivial task. There is, however, an analytic solution for $v_i(\boldsymbol{r})$ for a special case, to wit when the electrodes take the shape of the SVEL balance (figure 1*h*). We will use this shape to obtain an order-of-magnitude estimate of the effect of a charged particle for an arbitrary balance shape.

To find $v_i(\boldsymbol{r})$ for the SVEL shape, the potential inside a grounded conducting sphere

containing a particle of charge q must be obtained. This is easily done using the method of images (see, for example, Jackson 1975). The electric field at position $\boldsymbol{r}$ inside the sphere when the particle is at $\boldsymbol{r}$ is

$$\boldsymbol{E}_{\mathrm{i}}(\boldsymbol{r}) = \frac{1}{4\pi\epsilon_0}\frac{(q/z_0^2)\,(z_0/r_{\mathrm{s}})^3}{[1-(z_0/r_{\mathrm{s}})^2]^2}\boldsymbol{e}_s, \tag{A 1}$$

where z_0 is in this case the radius of the sphere. Since $\boldsymbol{E}_{\mathrm{i}}(\boldsymbol{r})$ depends only on r_{s}, it has no odd parity component, and only the even parity component of the field is affected. By using the same non-dimensionalization as for $\boldsymbol{E}_+$, we obtain

$$\boldsymbol{\Xi}_{\mathrm{i}}(\boldsymbol{r}) = \frac{1}{4\pi\epsilon_0}\frac{(q/v_{\mathrm{ring}}\,z_0)\,(z_0/r_{\mathrm{s}})^3}{[1-(z_0/r_{\mathrm{s}})^2]^2}\boldsymbol{e}_s. \tag{A 2}$$

Expanding (A 2) in powers of r_{s}, we obtain

$$\boldsymbol{\Xi}_{\mathrm{i}}(\boldsymbol{r}) = \frac{1}{4\pi\epsilon_0}\frac{q}{v_{\mathrm{ring}}\,z_0}\left(\frac{r_{\mathrm{s}}}{z_0}+\ldots\right)\boldsymbol{e}_s. \tag{A 3}$$

Comparing this result with our previous expression (23) for $\boldsymbol{\Xi}_+$ in the limit of small perturbations, we see that the relative error in $\boldsymbol{\Xi}_+$ is of order $q/(4\pi\epsilon_0\,v_{\mathrm{ring}}\,z_0\,C_1)$. Typical values are C_1 of order 1, z_0 of order 1 cm, and v_{ring} of order 1000 V. For values of q on the order of one electron charge, the relative error for such a case is on the order of 10^{-10}. The error becomes significant for sufficiently large q values.

Appendix B

The purpose of this Appendix is to prove the statements made in §4*a* about how to optimize a potential-limited electrodynamic balance for levitation or for stability, for an arbitrary excluded volume. It was shown in §4*a* that the optimum shapes for levitation and stability are obtained by maximizing $|D_0|$ and $|D_1|$ respectively. The design constants D_0 and D_1 are proportional to the series coefficients c_0 and c_1 in the expansion for v. Stated in terms of the dimensionless components of v, we will show that the optimum balance for levitation is obtained with

(i) $V_- = 1$ on portions of the surface S_{e} of the excluded volume for which $0 < \theta < \frac{1}{2}\pi$ and

(ii) $V_- = -1$ on portions of S_{e} for which $\frac{1}{2}\pi < \theta < \pi$,

while the optimum balance for stability is obtained with

(iii) $V_+ = 1$ on portions of S_{e} for which $\theta_1 < \theta < \pi - \theta_1$ and

(iv) $V_+ = 0$ on portions of S_{e} for which $0 < \theta < \theta_1$ or $\pi - \theta_1 < \theta < \pi$.

To prove this, we will find expressions for the series coefficients c_0 and c_1 in terms of the potential components on the surface of the excluded volume, find the potentials that maximize $|c_0|$ and $|c_1|$, and demonstrate that they are equal to the potentials described above. It should be noted that the electrodes must completely enclose the excluded volume to obtain the above potentials; the optimum balance shape is the same as the excluded volume shape.

The equivalent of (1) in integral form is

$$v(\boldsymbol{r}) = \frac{1}{4\pi\epsilon_0}\int\frac{\rho(\boldsymbol{r}')\,\mathrm{d}^3\boldsymbol{r}'}{|\boldsymbol{r}'-\boldsymbol{r}|}, \tag{B 1}$$

where the integration must be carried out over a volume that contains all of the charge. In an electrodynamic balance, the charges are confined to the surface of the

electrodes, so the right-hand side of (B 1) reduces to an integral over the electrode surfaces. These surfaces must be either on the surface S_e of the excluded volume or outside the excluded volume. Applying potentials to the electrodes yields a unique solution $v(\boldsymbol{r})$ and unique surface charge distributions on the electrodes. In general, one solves for $v(\boldsymbol{r})$ in a volume that includes all regions outside the electrodes, and this volume does not necessarily coincide with the excluded volume, but for this proof, it is convenient to concentrate on the excluded volume only. The potential everywhere inside the excluded volume is determined if the potential is known on S_e. The potential on S_e may be thought of as being established by a large number of fiducial conductors, each of infinitesimal area and each with an independently applied potential and induced charge density. All of the charge is then confined to S_e, so that, in the continuum limit, (B 1) becomes a surface integral of surface charge density over S_e:

$$v(\boldsymbol{r}) = \frac{1}{4\pi\epsilon_0}\int_{S_e}\frac{\sigma(\boldsymbol{r}')\,\mathrm{d}S'}{|\boldsymbol{r}'-\boldsymbol{r}|}. \tag{B 2}$$

To obtain expressions for c_0 and c_1, one can use the fact that, according to (5), $c_0 = \partial v(0)/\partial z$ and $c_1 = \frac{1}{2}\partial^2 v(0)/\partial z^2$. Taking partial derivatives of (B 2) and setting $\boldsymbol{r} = 0$ gives expressions for c_0 and c_1 of the form

$$c_j = \frac{1}{4\pi\epsilon_0}\int_{S_e} f_j(\boldsymbol{r})\,\sigma(\boldsymbol{r})\,\mathrm{d}S, \tag{B 3}$$

with

$$f_0(\boldsymbol{r}) = \frac{z}{(r^2+z^2)^{\frac{3}{2}}}, \quad f_1(\boldsymbol{r}) = \frac{z^2-\frac{1}{2}r^2}{(r^2+z^2)^{\frac{5}{2}}}. \tag{B 4}$$

The function $f_0(\boldsymbol{r})$ is positive for $z > 0$ and negative for $z < 0$; in terms of the polar angle θ, $f_0(\boldsymbol{r})$ is positive for $\theta < \frac{1}{2}\pi$ and negative for $\theta > \frac{1}{2}\pi$. Similarly, $f_1(\boldsymbol{r})$ is positive for $\theta < \theta_1$ or $\theta > \pi-\theta_1$ and negative for $\theta_1 < \theta < \pi-\theta_1$. Hence c_0 is maximized when $\sigma(\boldsymbol{r})$ is as large as possible for $\theta < \frac{1}{2}\pi$ and as small as possible for $\theta > \frac{1}{2}\pi$. Likewise, c_1 is minimized when $\sigma(\boldsymbol{r})$ is as small as possible for $\theta < \theta_1$ or $\theta > \pi-\theta_1$ and as large as possible for $\theta_1 < \theta < \pi-\theta_1$. Since the design places constraints on $v(\boldsymbol{r})$ rather than $\sigma(\boldsymbol{r})$, a relation between σ and v must be found.

If $v(\boldsymbol{r})$ is known on S_e, $\sigma(\boldsymbol{r})$ is determined on S_e, and conversely. The electric field on the surface of a conductor is also determined by σ, as $\boldsymbol{E} = (\sigma/\epsilon_0)\,\boldsymbol{n}$. Use of this fact and (2) gives

$$\partial v/\partial n = -\sigma/\epsilon_0 \tag{B 5}$$

on the surface of the conductor. Equation (B 5) contains the information needed about the relation between σ and v. To see this, we can first set $v = 0$ on all of the conductors on S_e except one, say conductor j, and then vary the potential v_j and surface charge σ_j on conductor j. When $v_j = 0$, the solution is $v = 0$ everywhere, so that $\partial v/\partial n = 0$ on j and hence $\sigma_j = 0$. When $v_j > 0$, conductor j is at the maximum v, so $(\partial v/\partial n)_j \leqslant 0$ on j and hence $\sigma_j \geqslant 0$. When $v_j < 0$, similarly, j is at the minimum v, so $(\partial v/\partial n)_j \leqslant 0$ and hence $\sigma_j \geqslant 0$. Linearity, in point of fact, requires that

$$(\partial v/\partial n)_j = -\chi_j v_j \tag{B 6}$$

for some proportionality constant χ_j. It is evident from the above considerations that $\chi_j \geqslant 0$. Substitution of (B 5) into (B 6) gives

$$\chi_j v_j = \sigma_j/\epsilon_0. \tag{B 7}$$

The product $\chi_j \epsilon_0$ is a positive definite capacitance per unit area.

We can now generalize the above results to the case of arbitrary potentials imposed on the rest of the conductors by adding a second potential $v'(\boldsymbol{r})$ that gives the desired values on the rest of the conductors but equals zero on j. When this potential is superposed on the first potential, another term enters into (B 6), with the result

$$\sigma_j = \chi_j \epsilon_0 v_j + \epsilon_0 (\partial v'/\partial n)_j. \tag{B 8}$$

Since $\chi_j \epsilon_0$ is positive definite, σ_j is maximized by maximizing v_j. We conclude that (i) c_0 is maximized when $v(\boldsymbol{r})$ is as large as possible for $\theta < \frac{1}{2}\pi$ and as small as possible for $\theta > \frac{1}{2}\pi$ and (ii) c_1 is minimized when $v(\boldsymbol{r})$ is as small as possible for $\theta < \theta_1$ or $\theta > \pi - \theta_1$ and as large as possible for $\theta_1 < \theta < -\theta_1$. When $v(\boldsymbol{r})$ is resolved into its even and odd parity components V_+ and V_-, maximizing c_0 requires an odd parity potential (so that $V_+ = 0$) and maximizing c_1 requires an even parity potential (so that $V_- = 0$). By using the definition of V_- and the fact that $-1 < V_- < 1$, we find that to optimize c_0 we require that on S_e, V_- must be given by

$$V_- = \begin{cases} 1 & \text{for} \quad 0 < \theta < \frac{1}{2}\pi \\ -1 & \text{for} \quad \frac{1}{2}\pi < \theta < \pi. \end{cases} \tag{B 9}$$

Likewise, using the definition of V_+ and the fact that $0 < V_+ < 1$, we find that to optimize c_1 we require that on S_e, V_+ must be given by

$$V_+ = \begin{cases} 0 & \text{for} \quad 0 < \theta < \theta_1, \\ 1 & \text{for} \quad \theta_1 < \theta < \pi - \theta_1, \\ 0 & \text{for} \quad \pi - \theta_1 < \theta < \pi. \end{cases} \tag{B 10}$$

Since the design constants appropriate to the excluded volume will be proportional to c_0 and c_1, (B 9) and (B 10) optimize the design constants as well.

References

Arnold, S. & Hessel, N. 1985 *Rev. scient. Instrum.* **56**, 2066–2069.

Arnold, S. & Folan, L. M. 1987 *Rev. scient. Instrum.* **58**, 1732–1735.

Ataman, S. & Hanson, D. N. 1969 *Ind. Eng. Chem. Fundam.* **8**, 833–836.

Berg, T. G. O. & Gaukler, T. A. 1969 *Am. J. Phys.* **37**, 1013–1018.

Berg, T. G. O., Trainor, R. J., Jr & Vaughan, U. 1970 *J. atmos. Sci.* **27**, 1173–1181.

Courant, E. D., Livingston, M. S. & Snyder, H. S. 1952 *Phys. Rev.* **88**, 1190–1196.

Davis, E. J. 1983 *Aerosol Sci. Technol.* **2**, 121–144.

Davis, E. J. 1985 *Langmuir* **1**, 379–387.

Davis, E. J. 1987 In *Surface and colloid science* (ed. E. Matijević), vol. 14, pp. 1–81. New York: Plenum Press.

Davis, E. J., Ward, T. L., Rodenhizer, D. G., Jenkins, R. W. & McRae, D. D. 1988 *Part. Sci. Technol.* **6**, 169–180.

Davis, E. J., Buehler, M. F. & Ward, T. L. 1990 *Rev. scient. Instrum.* **61**, 1281–1288.

Fischer, E. 1959 *Z. Phys.* **156**, 1–26.

Frickel, R. H., Shaffer, R. E. & Stamatoff, J. B. 1978 *Chambers for the electrodynamic containment of charged aerosol particles*, report AD/A056 236. U.S. Department of Commerce, Springfield, Virginia: National Technical Information Service.

Good, M. L. 1953 *A proposed particle containment device*, report No. 4146. Livermore, California: University of California Radiation Laboratory (declassified 1956).

Hartung, W. H. & Avedisian, C. T. 1990 *The electrodynamic balance*, report No. E-90-04. Cornell University, Ithaca, New York: Department of Mechanical and Aerospace Engineering.

Jackson, J. D. 1975 *Classical electrodynamics*, 2nd edn. New York: John Wiley & Sons.

Maxwell, J. C. 1892 *A treatise on electricity and magnetism*. Oxford: Clarendon Press.

Millikan, R. A. 1917 *The electron, its isolation and measurement and the determination of some of its properties*. University of Chicago Press.

Müller, A. 1960 *Annln Phys.* **6**, 206–220.

Paul, W. & Raether, M. 1955 *Z. Phys.* **140**, 262–273.

Philip, M. A. 1981 An absolute method for aerosol particle mass measurement. MS thesis, Massachusetts Institute of Technology, U.S.A.

Philip, M. A., Gelbard, F. & Arnold, S. 1983 *J. Colloid Interface Sci.* **91**, 507–515.

Phuoc, T. X. & Maloney, D. J. 1988 In *Proc. 22nd Symp. (Int.) on Combustion*, pp. 125–134. New York: The Combustion Institute.

Richardson, C. B. & Spann, J. F. 1984 *J. Aerosol Sci.* **15**, 563–571.

Richardson, C. B., Lin, H.-B., McGraw, R. & Tang, I. N. 1986 *Aerosol Sci. Technol.* **5**, 103–112.

Sageev, G., Flagan, R. C., Seinfeld, J. H. & Arnold, S. 1986 *J. Colloid Interface Sci.* **113**, 421–429.

Schweizer, J. W. & Hanson, D. N. 1971 *J. Colloid Interface Sci.* **35**, 417–423.

Sloane, C. S. & Elmoursi, A. A. 1987 In *Conference record of the 1987 IEEE industry applications society annual meeting*, part II, pp. 1568–1577. New York: IEEE Publishing.

Spjut, R. E., Bar-Ziv, E., Sarofim, A. F. & Longwell, J. P. 1986 *Rev. scient. Instrum.* **57**, 1604–1610.

Straubel, E. & Straubel, H. 1986 In *Physical and chemical characterisation of individual airborne particles* (ed. K. R. Spurney), pp. 127–160. Chichester: Ellis Horwood.

Straubel, H. 1955 *Naturwissenschaften* **42**, 506–507.

Straubel, H. 1956 *Z. Elektrochem.* **60**, 1033–1036.

Ward, T. L. 1989 Radioactivity measurement of single microparticles using an electrodynamic balance. Ph.D. thesis, University of Washington, Seattle, U.S.A.

Ward, T. L., Davis, E. J., Jenkins, R. W. & McRae, D. D. 1989 *Rev. scient. Instrum.* **60**, 414–421.

Warren, J., Boicourt, G., Cooper, R., Menzel, M. & Stokes, H. 1987 *Reference manual for the POISSON/SUPERFISH group of codes*, report No. LA-UR-98-126. Los Alamos, New Mexico: Los Alamos National Laboratory.

Weiss-Wrana, K. 1983 *Astron. Astrophys.* **126**, 240–250.

Wineland, D. J., Itano, W. M. & Van Dyck, R. S., Jr 1983 *Adv. At. Mol. Phys.* **19**, 135–185.

Winslow, A. M. 1967 *J. Comput. Phys.* **2**, 149–172.

Wuerker, R. F., Shelton, H. & Langmuir, R. V. 1959 *J. appl. Phys.* **30**, 342–349.

Received 1 February 1991; revised 1 July 1991; accepted 14 October 1991